Fast Electron Transfer Across Semiconductor−Molecule Interfaces: GaAs/$Co(Cp)_2^{+/0}$

Andreas Meier,* Donald C. Selmarten, Kerstin Siemoneit,† Barton B. Smith,* and Arthur J. Nozik*

Center for Basic Sciences, National Renewable Energy Laboratory, 1617 Cole Boulevard, Golden, Colorado 80401

Received: July 30, 1998; In Final Form: January 20, 1999

The kinetics of majority electron transfer in the dark from n-GaAs electrodes to cobaltocenium ($Co(Cp)_2^+$) acceptors in acetonitrile has been studied in detail, both experimentally and theoretically. The experimental results were obtained from electrochemical impedance spectroscopy, quartz crystal microbalance (QCM and EQCM) studies, and current−potential characteristics. The theoretical work involved calculating the adsorption energy and molecular configuration of the cobaltocenium acceptors at the GaAs surface using high level density functional theory (B3LYP and variations thereof) as well as semiempirical methods. The QCM experiments showed that both $Co(Cp)_2^+$ and $Co(Cp)_2^0$ are physisorbed at GaAs surfaces, with adsorption energies of about 0.2 and 0.4 eV, respectively. The theoretical results are consistent with these experimental results. They indicate that adsorption of the $Co(Cp)_2^{+/0}$ redox system occurs on GaAs, with $Co(Cp)_2^0$ somewhat more strongly adsorbed than $Co(Cp)_2^+$; the $Co(Cp)_2^{+/0}$ molecules were found to adsorb with the cyclopentadienyl rings parallel to the GaAs surface. A model for the overall electron-transfer process was developed that incorporates $Co(Cp)_2^+$ adsorption. Analysis of the detailed impedance spectra over the range of 1 Hz to 600 kHz showed that the sequential electron-transfer steps in the model (i.e., electron transfer from the GaAs conduction band to adsorbed $Co(Cp)_2^+$, followed by electron transfer from the adsorbed $Co(Cp)_2^0$ to free $Co(Cp)_2^+$ in solution) are very fast and that the observed overall rate of electron transfer is limited by the rate of thermionic emission from the GaAs bulk region to the surface. The implications of these results for the theory of electron transfer at semiconductor−liquid interfaces, and the associated controversies surrounding theory and various experimental results for GaAs−metallocenium systems, are discussed.

I. Introduction

The kinetics of charge transfer at semiconductor−molecule interfaces (SMI) (also commonly referred to as semiconductor−electrolyte interfaces) is a very important issue that is currently receiving much attention.[1−13] The charge transfer can involve either electrons residing in the conduction band or positive holes residing in the valence band of the semiconductor; in this work we will only discuss electron transfer from the conduction band. Furthermore, the electron transfer (ET) can be from the semiconductor to redox acceptor molecules at the semiconductor surface, or it can involve electron injection from photoexcited adsorbed molecules into the semiconductor conduction band.[14−20] Finally, the former process includes electron transfer in the dark from n-type semiconductors (majority electron transfer) as well as photoinduced electron transfer from p-type semiconductors (minority electron transfer). Here, we will only discuss our work on the dark electron transfer of majority electrons from n-type semiconductors to redox acceptors. The acceptor species is the cobaltocenium cation in acetonitrile (ACN); the semiconductor is epitaxially grown GaAs.

ET kinetics are important both from the point of view of photoelectrochemical devices and for the fundamental science of these interfaces. For example, the efficiency of photoelectrochemical energy conversion systems depends on the rate of ET compared to the rates of electron−hole recombination at the surface and in the semiconductor bulk. Also, the possibility of hot electron transfer[1,3,21,22] from semiconductors to liquid redox electrolyte, and its associated beneficial effect on energy conversion efficiency,[23] depends on the rate of ET being faster than the rate of hot electron relaxation (i.e., cooling) via electron−phonon interactions.[22]

The dynamics of electron transfer across semiconductor-electrolyte interfaces is controversial, both with respect to theory and experiment. One approach to the theory has been to adapt a model that was developed for ET between two immiscible liquids[24,25] (which treats the redox species as hard spheres with fixed radii) to the semiconductor−liquid interface by modeling electrons in the semiconductor as hard spheres with a radius related to the Bohr radius of an electron bound to an impurity donor site in the semiconductor.[10] This model is constrained to the regime of nonadiabatic ET, i.e., to very weak electronic coupling between the semiconductor and the acceptor molecule and thus to nonadsorbing and ideal outersphere acceptors. The model has been challenged[26] and defended.[4−9] Experimental studies of ET kinetics have also been reported that both support[4−10] and apparently contradict[1,2,13] the theoretical predictions of this model.

The range of experimental results on the kinetics of ET at various semiconductor−liquid interfaces is very large, with the reported heterogeneous second-order rate constants (k_{ET}) varying by up to 6−7 orders of magnitude. The model proposed in refs 4−9 places an upper limit of about 1×10^{-17} cm^4/s for the rate constant for ET to nonadsorbed outersphere redox acceptors at semiconductor surfaces; this is presented as a general limit that is valid for all semiconductors and outersphere redox molecules. Experimental results reported in refs 4−10 are apparently consistent with this proposed upper limit. However,

† Institut für Solarenergieforschung, Hannover, Germany.

10.1021/jp983230x CCC: $18.00
Published on Web 03/11/1999

values of k_{ET} reported in refs 2 and 13 range from 1×10^{-10} to 1×10^{-18} cm^4/s; these values are based on the assumption that the acceptor concentration is the value for the bulk solution.

In this study we examine the reasons for the apparent discrepancy in reported k_{ET} values. We use quartz crystal microbalance (QCM) techniques, detailed impedance spectroscopic studies at low and high current flow, and theoretical calculations to examine the ET dynamics. We find that adsorption of the cobaltocenium redox acceptor plays a critical role in the dynamics, notwithstanding the general previous belief that metallocenes and their cations are outersphere, nonadsorbing molecules.[6,8,10,27,28] These results have important implications for the various models of ET at the SLI.

II. Experimental Section

A. Chemicals and Electrodes. The cobaltocene−cobaltocenium redox couple used in the electrochemical investigations was purchased from Strem Chemicals. Prior to use, the cobaltocene ($Co(Cp)_2^0$) was purified through sublimation in a vacuum at 70 °C and the cobaltocenium ($Co(Cp)_2^+$) hexafluorophosphate was recrystallized from ethanol. The acetonitrile (ACN, Burdick & Jackson) was refluxed for 1 day and distilled under nitrogen atmosphere over calcium hydride. Tetrabutylammonium hexafluorophosphate ($TBAPF_6$, Aldrich) was used as supporting electrolyte after it was recrystallized from ethanol three times and dried under vacuum at 180 °C. In all electrochemical studies the $TBAPF_6$ concentration of the ACN solutions was 0.3 M. All chemicals were stored in a glovebox under an atmosphere of helium gas.

The GaAs electrodes used for the electrochemical investigations presented here consist of a 2-μm-thick epilayer of GaAs grown on heavily doped GaAs substrates. The GaAs epilayers were grown in an atmospheric pressure metallorganic chemical vapor deposition (MOCVD) reactor. The doping density of the GaAs samples ranged between 1×10^{17} and 2×10^{17} cm^{-3} for the studies presented in this paper. For the electrochemical studies the GaAs epilayers were cut into small square pieces ($\approx 0.6 \times 0.6$ cm), contacted with Ga−In alloy, and mounted with conductive silver epoxy (Epoxy-Technology, 415G or H31) as rotating disk electrodes. To provide an approximately circular geometry of the electrode surface and to seal the electrodes, the edges of the GaAs epilayer were covered with Epoxy (HYSOL Epoxi-Patch). The electrode areas were usually between 0.23 and 0.15 cm^2. Prior to the experiments the electrodes were either treated with a half-concentrated HCl or half-concentrated NH_4OH solution for 60 s to remove gallium or arsenate oxides from the GaAs surface that developed during the preparation procedure. These etching procedures produced the highest rates of ET. GaAs electrode samples that had been sitting in air for several days and were unetched, or had been exposed to an oxidizing etch like $H_2O/H_2SO_4/H_2O_2$, showed slower ET rates by up to 6 orders of magnitude. The slow ET rates are attributed to oxide barrier layers on the surface.

The reference potential (measured with a platinum wire) was either the solution redox potential or the redox potential of a ferrocene−ferrocenium solution ($Fc^{+/0}$, molar ratio 1:1) separated by two frits (glass and "Vycor") in a different cell compartment. The counter electrode was a circular bent platinum wire placed on the flat bottom of the cone shaped cell.

B. Electrochemical Apparatus. The electrochemical measurements were performed in a glovebox (Mbraun, Labmaster 130) under an atmosphere of helium gas and using a three-electrode setup. Current−voltage (I−V) and impedance spectroscopic measurements (1 Hz to 600 kHz) were performed using a Solartron 1260-FRA in conjunction with a Solartron 1287-EI potentiostat. To avoid artifacts in impedance measurements in the high-frequency range (>50 kHz), the platinum wire of the reference electrode was short circuited via a capacitance (10 nF) and a platinum wire in series.[29] Only the tip of the platinum wire was exposed to the cell solution and placed close to the frit of the reference electrode. The majority of experiments were conducted at rotating disk electrodes (RDE) at rotation velocities between 50 and 2000 rpm (Rotator AFASR, Pine Instrument).

C. Quartz Crystal Microbalance (QCM). The QCM allows in situ detection of mass changes at an electrode surface with submonolayer precision; it is actually a quartz crystal nanobalance. The basis for the QCM's mass sensitivity is the piezoelectric effect for materials that crystallize with noncentrosymmetric space groups; an electric potential causes a physical distortion of the crystal lattice. A crystal of given mass will resonate at a specific frequency. The resonant frequency is determined by the acoustic properties of the particular crystal. Changes in crystal mass or thickness (e.g., from adsorption of material from solution or vapor deposition) result in a change in the resonant frequency. This frequency change is described by the Sauerbrey equation:

$$\Delta f = -\frac{2f_0^2 \Delta m}{A(\rho_q \mu_q)^{1/2}} \quad (1)$$

where Δf is the measured frequency change, f^0 is the fundamental frequency of the oscillator, Δm is the change of mass, A is the piezoelectrically active area, ρ_q is the density of quartz (2.648 g cm^{-3}), and μ_q is the shear modulus for quartz (2.947×10^{11} dyn cm^{-2}).[30]

The quartz crystal nanobalance instrument used in the measurements was an Elchema model EQCN-700. When electrochemical experiments were performed, the above instrument was used in conjunction with an Elchema Model PS-605 high-precision potentiostat/galvanostat. The working electrode was the GaAs epilayer (with potential necessarily held at ground), and Pt wires were used for the counter and reference electrodes. The 10 MHz quartz crystals were obtained from International Crystal Manufactures. The crystals were first cleaned with dichloromethane to remove any organic contaminants prior to use.

In order for the mass sensitive surface to consist of GaAs, it was necessary to position a piece of single crystal GaAs onto the active surface of the nanobalance crystal. Since GaAs could not be epitaxially grown directly onto a substrate of gold, the following procedure was performed. A multiepilayer structure was prepared with the intention of removing all material but the epilayer of interest from the structure and introducing this epilayer onto the nanobalance crystal. The initial multilayered structure consisted of a substrate of bulk GaAs, a stop-etch layer of 1 μm of $GaInP_2$, and a 1 μm epilayer of GaAs. The stop layer and the GaAs epilayer of interest were grown epitaxially in an MOCVD reactor. This device was then placed (epilayer down) in black wax in order to protect it from etching. The substrate was then etched with a solution of phosphoric acid/peroxide/water (3:4:1), which effectively removed the bulk GaAs, but was unreactive to $GaInP_2$ (the stop-etch layer). The $GaInP_2$ stop-etch layer was then removed by a hydrochloric acid/acetic acid/peroxide (2/20/1) solution. This solution was chosen for its selective reactivity toward $GaInP_2$ over GaAs. With only the epitaxial GaAs remaining, a thin layer of Au (400 Å) was added by vapor deposition. This was accomplished in a Key

High Vacuum Products model KV-301 gold evaporator (base line pressure 1×10^{-6} Torr). This gold layer was added to improve the nanobalance/GaAs contact and to provide ohmic contact to the circuit. The black wax was removed from the GaAs epilayer with dichloromethane, and the epilayer was then "floated" onto the quartz crystal. Edges of the GaAs and any exposed gold were then coated with protective nylon (solvated in phenol). Because the 10 MHz crystals are physically too fragile to be used in reusable cells in conjunction with O-rings, the nanobalance crystal with the GaAs epilayer was permanently glued with silicone to a glass cell, with the epilayer facing the solution side of the cell. The QCM measurements were made both at open circuit (no current flow), and with current flow to determine if there are mass changes associated with ET and faradaic current. With current flow QCM is referred to as an electrochemical quartz crystal Microbalance (EQCM) experiment.

If the electrode shows a weight increase during current flow, then ET has caused either (a) adsorption of the reduced acceptor species or (b) multilayer formation of the reduced acceptor (if the acceptor was already adsorbed prior to current flow). If there is a weight loss during current flow, then ET has resulted in a desorption of the reduced acceptor species. Finally, if there is no change in electrode mass, then (a) the ET is mediated either through a self-exchange reaction between adsorbed and free acceptors in solution or (b) the rate of desorption and adsorption are comparable.

D. Blank Preparation. SiO_2 was deposited onto a nanobalance crystal by e^- beam evaporation. The resistive quality of the overlayer was tested with an I−V experiment. The gold blank was prepared by vapor depositing approximately 500 angstroms of gold onto the quartz crystal in a gold evaporator (Key High Vacuum Products model KV-301). For the nylon blank, nylon suspended in a volatile organic matrix was simply applied to the surface of the quartz crystal; it was then cured at elevated temperatures. In this case the integrity (insulating value) of the nylon coverage was tested with an I−V experiment. In all cases the treated nanobalance crystals were glued to a glass cell with silicone.

Viscosity measurements were performed with a Cannon−Ubbelolde viscometer, model 25 B114. The average of at least five room-temperature measurements was taken to be the kinematic viscosity for a given solution concentration of analyte.

III. QCM Results

A. Cobaltocenium Response. As can be seen in Figure 1a, GaAs shows a mass response to changes in the solution concentration of cobaltocenium. An electrode mass change (when it has been experimentally verified that there is no viscosity change) indicates that cobaltocenium is binding to the surface of the GaAs electrode. The supporting electrolyte in this experiment is 100 mM $TBAPF_6$; this was chosen to most closely match the experimental conditions in the electrochemical experiments. In other experiments, the addition of two aliquots of blank electrolyte solution was investigated to ascertain the systems susceptibility to the mechanical stresses of aliquot addition. Although the system did show a slight perturbation to the mechanical addition of electrolyte, it was seen that this is a transient response and that the equilibrium resonant frequency was quickly reestablished. This method of adding a blank solution to the QCM cell has been similarly employed in the literature[31] to establish unequivocally that the analyte was binding to the electrode.

B. Cobaltocene Response. As seen in Figure 1b, addition of the neutral cobaltocene species to the cell also evokes a mass change at the GaAs electrode.[32] Note that in this figure the scale is an order of magnitude larger than the cobaltocenium case, and the concentration of the added species is several times more dilute. This indicates qualitatively that while both oxidized and reduced forms of the redox species display an affinity for the GaAs surface, the neutral reduced species is bound more strongly. In fact, in our preliminary experiments, cobaltocene additions after the initial aliquot render only minor mass inflections. This behavior suggests that a monolayer may have formed with the initial addition of cobaltocene. This monolayer formation may have an inhibiting effect on further binding events.

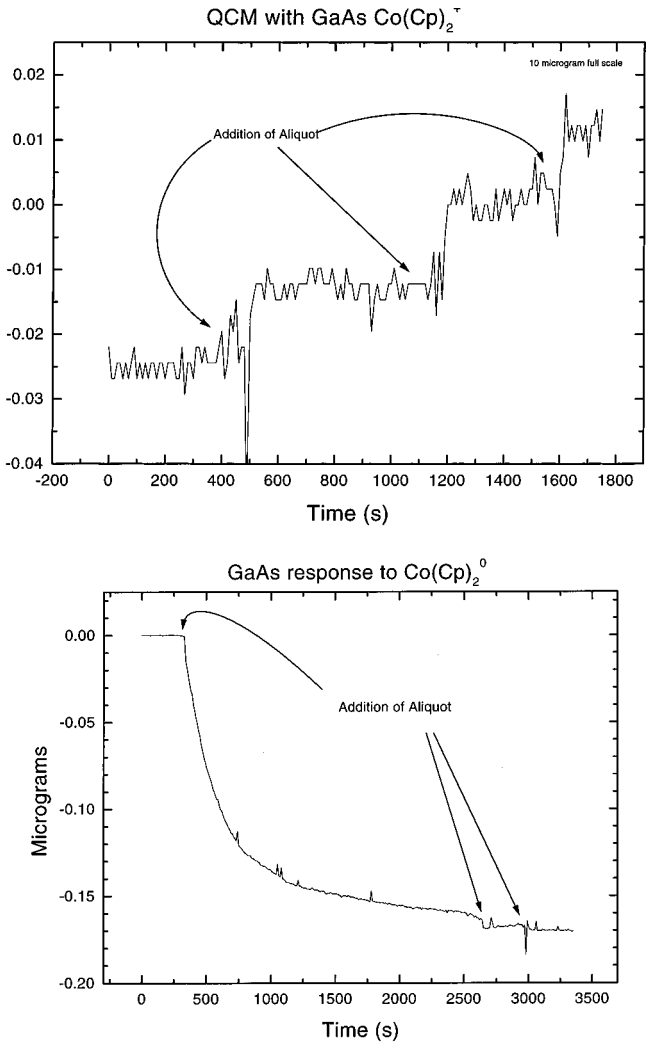

Figure 1. (a) QCM response of GaAs upon the addition of aliquots of 5 μL of 100 mM $Co(Cp)_2^+$ in ACN to a cell containing 1 mL of electrolyte (100 mM $TBAPF_6$ in ACN). (b) QCM response of GaAs upon the addition of aliquots of 5 μL of 44 mM $Co(Cp)_2^0$ in ACN to 3 mL of electrolyte.

C. EQCM Results. With current flow the quartz crystal electrode showed no change in mass even as the diffusion-limited current was approached (potential more negative than −320 mV) (see Figure 2). When the current was driven at the highest values (in a galvanostatic experiment), a mass change could be observed after tens of seconds. Concurrent with this mass change was a dramatic shift of potential (more than 800 mV). On the basis of literature reports of cobaltocene reduction of platinum microelectrodes,[33] we believe this mass change at high potential and current to be associated with the further reduction of neutral cobaltocene and subsequent adsorption.

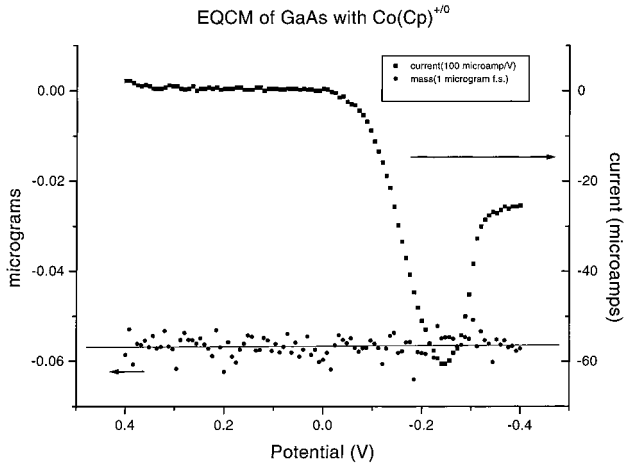

Figure 2. EQCM response (mass and current) of n-GaAs as a function of electrode potential. Electrolyte is 100 mM $TBAPF_6$ with 0.33 mM $Co(Cp)_2^+$ and 0.03 mM $Co(Cp)_2^0$.

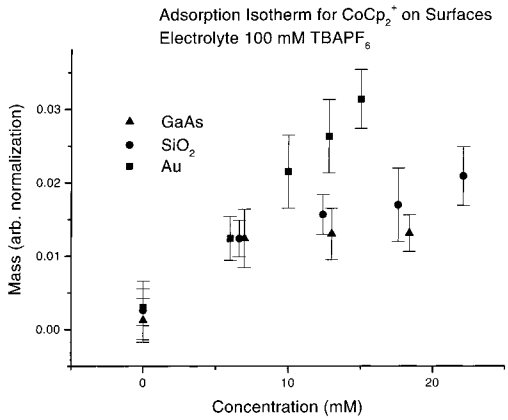

Figure 3. Comparison of adsorption isotherms for $Co(Cp)_2^+$ on GaAs, SiO_2, and Au surfaces.

Whereas this reaction is not directly involved with the scope of this paper, it is interesting that we are able to observe it with EQCM.

D. Blanks. To verify that the results in our experiments were exclusively from activity at the GaAs−electrolyte interface, we performed several control experiments. In each case we configured the cell in such a way that only one material was exposed to solution. Each material was chosen to represent any possible surface that may be exposed to the electrolyte solution in the actual GaAs experiment. Figure 3 shows the response from the different blanks (and GaAs) to changing solution concentration of $Co(Cp)_2^+$. The first thing to note is that all surfaces (except nylon, not shown) show some affinity for the cobaltocenium species. Whereas each surface (except for nylon) does show a response, each isotherm is different in both shape and slope. Au shows a linear mass response with changing solution concentration. A linear isotherm indicates physical adsorption with no monolayer distinction; i.e., the surface shows the same affinity for the solution species after an entire monolayer has been formed. This activity excludes the possibility that a chemical bond forms between the surface and the species. The response of SiO_2 to changing cobaltocenium concentrations has a much more shallow slope and displays a slight change in slope after the solution concentration reaches 10 mM. The different slopes indicate that cobaltocenium has a differentially higher affinity for gold than quartz. In contrast, the GaAs surface becomes relatively unresponsive to changes in solution concentrations greater than 10 mM. This experimental behavior indicates that, for cobaltocenium on GaAs, a monolayer of cobaltocenium is bound more strongly than any subsequently bound material.

It has been shown that changes in solution viscosity can have an effect on the resonant frequency of a QCM.[34] The contributions of solution viscosity (η_L) and density changes (ρ_L) are shown in eq 2. Here, f_s is the fundamental frequency of the crystal. Careful viscosity measurements exclude any significant viscosity changes within the concentration range of cobaltocenium used in these studies.

$$\Delta f_s = -[2f_s^2/(\mu_q\rho_q)^{1/2}][(\Delta m/A) + [\rho_L\eta_L/4\pi f_s]^{1/2}] \quad (2)$$

It is reasonable to assume that in our experiments, the mass change response is from the GaAs surface. In an AT cut piece of quartz there is a differential sensitivity constant, c_f:

$$c_f = df/dm = S \quad (3)$$

This represents the differential frequency change for a given mass change at a particular region of the crystal surface. That is, the change in frequency per unit mass is a function of position on the crystal. Essentially this sensitivity function looks like a Gaussian centered at the gold flag overlap regions and decreases monotonically to the point of being negligible beyond the electrode boundary. The instrument reads the integral sensitivity constant (the differential sensitivity constant integrated over the surface of the crystal) when it is measuring a frequency change. Energy trapping, the effect of the crystal oscillations being confined to a region of higher density (defined by the electrode region), tends to confine the oscillations of the quartz crystal in the region that has the gold electrodes deposited. Hence, considering that nylon is a nonresponsive material and coats everything but the exposed GaAs, the mass response observed in these experiments arises from the GaAs electrode−electrolyte interface.

E. Absorption Isotherm. *Langmuir Isotherm*. Thermodynamic information about the adsorption process may be obtained from the adsorption isotherms. The free energy of adsorption is defined as the difference in the standard electrochemical potentials between the adsorbed and free species, $\bar{\mu}_i^{0,A}$ and $\bar{\mu}_i^{0,b}$ respectively, as shown in eq 4.

$$\Delta\bar{G}_i^0 = \bar{\mu}_i^{0,A} - \bar{\mu}_i^{0,b} \quad (4)$$

A number of different isotherms have been proposed (logarithmic Temkin, Frumkin, etc.), and there have been a number of different experimentally determined isotherm shapes.[35] Here we use the simple Langmuir isotherm to interpret our experimental data. When employing this model, certain assumptions are involved; specifically, there is no interaction between adsorbed species on the electrode surface, the surface is completely uniform, and at high bulk activities a monolayer is formed. Although the Langmuir isotherm involves several assumptions, some of which are not precisely valid, and at best may be considered to be less than rigorous, it has been proven in the past to be a useful semiquantitative tool in the analysis of adsorption events:

$$\beta = \exp\left(\frac{-\Delta\bar{G}_i^0}{RT}\right) \quad (5)$$

$$\frac{\theta}{1-\theta} = \beta_i a^b{}_1 \quad (6)$$

In the above expressions, the free energy of adsorption is shown in terms of the fractional coverage of the surface, $\Gamma_i/\Gamma_s = \theta$. Where Γ_i is the surface excess of species i at equilibrium, and Γ_s is the surface excess of species i at saturation. The above expression can also be written in terms of solution concentration of species if the activity coefficients are included in the β term. In this simplistic treatment of the isotherm, we are not accounting for any competitively adsorbed/desorbed species in the QCM studies

$$\Gamma_i = \frac{\Gamma_s \beta_i C_i}{1 + \beta_i C_i} \tag{7}$$

In our analysis of the experimental isotherms for GaAs/Co(Cp)$_2^+$ (see Figure 4), we assume that monolayer coverage coincides with the first plateau of the electrode mass/solution concentration plot. At this inflection point, the change in the GaAs electrode mass equals 0.065 μg. This corresponds to 7.5 $\times$ 10^{13} molecules/cm^2 (or equivalently 1.15 nm separation from center to center). In an ideal close-packed surface (assuming a molecule diameter of 4.6 Å) the molecule density would be 4.7 $\times$ 10^{14} particles per cm^2. Since Co(Cp)$_2^0$ forms a monolayer on GaAs at much lower bulk solution concentrations (i.e., 0.1 mM), it is assumed that with both Co(Cp)$_2^0$ and Co(Cp)$_2^+$ present in the electrochemical experiments at 0.9 and 1.3 mM, respectively, a full monolayer of Co(Cp)$_2^{0/+}$ is present. This total coverage is taken to be approximately 4 $\times$ 10^{14} molecules/cm^2. As discussed in the next section, at equilibrium the ratio of the oxidized and reduced species will be the same as in the bulk solution.

Heiland, Gileadi, and Bockris have studied the adsorption of benzene on platinum;[36] they used a value of 1.5 $\times$ 10^{14} particles/cm^2 as one monolayer. Also, Shimazu et al. have reported the adsorption of a monolayer of ferrocenyldodecanethiol on gold that consisted of a density of 2.6 $\times$ 10^{14} molecules cm^{-2}.[31] Thus, the number we have used here for monolayer coverage seems reasonable. On the basis of the above Langmuir treatment of our adsorption data for Co(Cp)$_2^+$ on GaAs (see Figure 4), the free energy of adsorption is approximately 20 kJ/mol (0.2 eV); for Co(Cp)$_2^0$ the adsorption free energy is estimated to be 0.4 eV.

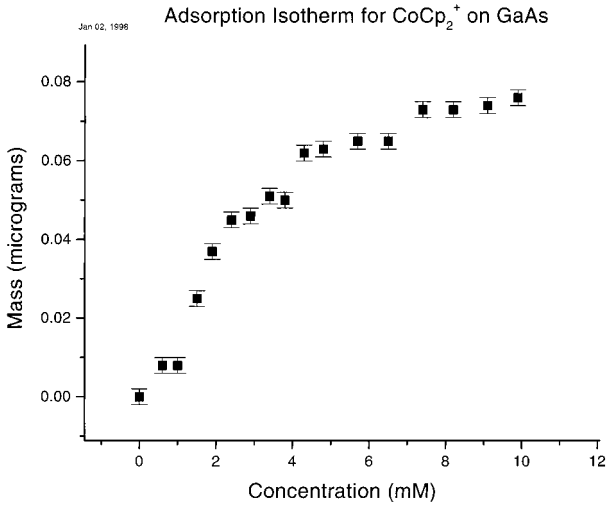

Figure 4. Adsorption isotherm for Co(Cp)$_2^+$ on GaAs.

IV. Impedance Measurements

A. Theory and Models. The kinetics of majority charge carrier (electron) transfer for the Co(Cp)$_2^{+/0}$ redox reaction at n-GaAs in ACN was previously studied and described based on a simple heterogeneous charge-transfer reaction and applying a second-order rate law.[2] For a second-order rate law the electron transfer rate is proportional to the concentration of the redox species and the electron density at the semiconductor surface. However, this model leads to an unusually large ET rate constant if the bulk concentration of Co(Cp)$_2^+$ is used in the analysis,[2] and it also does not satisfactorily describe all the experimental results. Further investigations reported here reveal that electron transfer between the n-GaAs electrode and the Co(Cp)$_2^{+/0}$ redox system in solution occurs via Co(Cp)$_2^{+/0}$ molecules that are adsorbed on the semiconductor surface.

Depending on the adsorption strength, it is reasonable to distinguish two parallel reaction mechanisms that occur after the first electron-transfer process from the semiconductor to the adsorbed redox molecules. These two mechanisms, illustrated in Figure 5, are (1) adsorption and desorption reactions of the redox molecules on the semiconductor surface and (2) a self-exchange (i.e., mediated ET) reaction between the adsorbed redox molecules and the redox species in solution.

Depending on the binding strength of the adsorbed redox molecules, either one of the two parallel mechanisms can become a rate-determining reaction. This will be the adsorption and desorption of the redox molecules if these reactions are much faster than the self-exchange. However, if the self-exchange rate is much faster than the adsorption and desorption processes, then the rate-determining reaction will be the self-exchange reaction between adsorbed cobaltocene−cobaltocenium molecules (Co(Cp)$_2^{+/0}$(ad)) and the cobaltocene−cobaltocenium molecules in solution (Co(Cp)$_2^{0/+}$(sol)).

To develop a model that describes the electrochemical current−voltage (I−V) and impedance behavior of the system, the charge-transfer steps have to be quantified. In the following, the chemical reactions and the corresponding expressions for the reactions rates are described

chemical reactions		reaction rates	
majority charge carrier transfer			
$Co(Cp)_2^{+}{}_{(ad)} + e^- \underset{k_c^+}{\overset{k_c^-}{\rightleftharpoons}} Co(Cp)_2^{0}{}_{(ad)}$	(8)	$R_c^- = N_{ad}^{max} k_c^- n_s \theta_{ox}$	(8a)
		$R_c^+ = N_{ad}^{max} k_c^+ N_c \theta_{red}$	(8b)
self-exchange reaction			
$Co(Cp)_2^{0}{}_{(ad)} + Co(Cp)_2^{+}{}_{(sol)} \underset{k_{se}^+}{\overset{k_{se}^-}{\rightleftharpoons}} Co(Cp)_2^{+}{}_{(ad)} + Co(Cp)_2^{0}{}_{(sol)}$	(9)	$R_{se}^- = N_{ad}^{max} k_{se}^- \theta_{red} c_{ox}^s$	(9a)
		$R_{se}^+ = N_{ad}^{max} k_{se}^+ \theta_{ox} c_{red}^s$	(9b)
adsorption and desorption reactions			
$Co(Cp)_2^{+}{}_{(ad)} \underset{k_{ox}^-}{\overset{k_{ox}^+}{\rightleftharpoons}} Co(Cp)_2^{+}{}_{(sol)}$	(10)	$R_{ox}^- = N_{ad}^{max} k_{ox}^- (1-\theta) c_{ox}^s$	(10a)
		$R_{ox}^+ = N_{ad}^{max} k_{ox}^+ \theta_{ox}$	(10b)
$Co(Cp)_2^{0}{}_{(ad)} \underset{k_{red}^+}{\overset{k_{red}^-}{\rightleftharpoons}} Co(Cp)_2^{0}{}_{(sol)}$	(11)	$R_{red}^- = N_{ad}^{max} k_{red}^- \theta_{red}$	(11a)
		$R_{red}^+ = N_{ad}^{max} k_{red}^+ (1-\theta) c_{red}^s$	(11b)

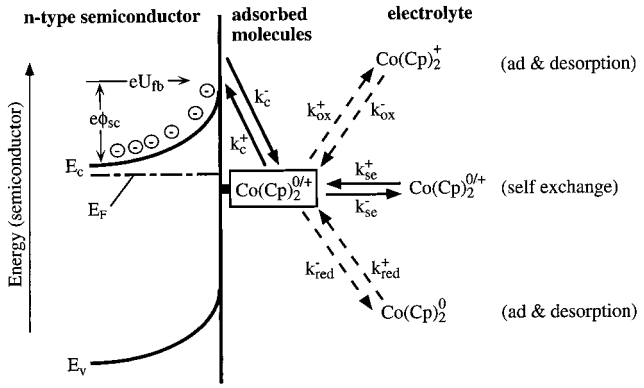

Figure 5. Energy diagram for an n-type semiconductor (left side) and kinetic reaction scheme for charge transfer to the $Co(Cp)_2^{+/0}$ redox couple in solution via adsorbed $Co(Cp)_2^{+/0}$ molecules (right side).

where R is the reaction rate; N_{ad}^{max} is the maximum number of adsorption sites, N_c is the effective density of states in the conduction band; θ_{red} is the degree of coverage of $Co(Cp)_2^0$; θ_{ox} is the degree of coverage of $Co(Cp)_2^+$; θ is the total degree of coverage of $Co(Cp)_2^0$ and $Co(Cp)_2^+$ ($\theta = \theta_{ox} + \theta_{red}$); n_s is the electron density at the semiconductor surface; c_{ox} and c_{red} are the concentrations of $Co(Cp)_2^+$ and $Co(Cp)_2^0$, respectively; and k are rate constants (k_c^-, k_c^+, k_{se}^-, k_{se}^+, k_{ox}^-, k_{red}^+ in $cm^3\ s^{-1}$ and k_{ox}^+, k_{red}^- in s^{-1}).

In the next section, the kinetic expressions that follow from eqs 8−11 are derived. Since the results of the QCM measurements show that $Co(Cp)_2^0$ is significantly more strongly adsorbed to GaAs than $Co(Cp)_2^+$, it is reasonable to assume that the self-exchange reaction is much faster than the adsorption and desorption processes and that the $Co(Cp)_2^+$ reduction therefore proceeds via the self-exchange reaction rather than via adsorption and desorption.

1. Charge Transfer via a Self-Exchange Reaction. The faradaic current for the majority charge carrier transfer across the semiconductor interface is obtained from the reaction rates (eq 8a and b). Considering that the reduction current is negative and the oxidation current positive, the expression for the faradaic current (I_F) is

$$I_F = e\,A(R_c^+ - R_c^-) = e\,A\,N_{ad}^{max}(k_c^+ N_c \theta_{red} - k_c^- n_s \theta_{ox}) \quad (12)$$

where e is the elementary charge and A is the area of the electrode surface.

The time-dependent occupation of the adsorption sites with oxidized and reduced redox molecules is defined by the mass and charge balance for the adsorption and desorption processes and the charge-transfer events (eq 13a−c).

$$N_{ad}^{max}\frac{d\theta}{dt} = R_{ox}^- - R_{ox}^+ - R_{red}^- + R_{red}^+ \quad (13a)$$

$$N_{ad}^{max}\frac{d\theta_{ox}}{dt} = R_{se}^- - R_{se}^+ - R_c^- + R_c^+ + R_{ox}^- - R_{ox}^+ \quad (13b)$$

$$N_{ad}^{max}\frac{d\theta_{red}}{dt} = R_{se}^+ - R_{se}^- - R_c^+ + R_c^- + R_{red}^+ - R_{red}^- \quad (13c)$$

Equations 13a−c include the assumption that the $Co(Cp)_2^+$ and $Co(Cp)_2^0$ molecules adsorb at the same kind of adsorption sites on the semiconductor surface, i.e., for stationary conditions

$$\theta = \theta_{ox} + \theta_{red} \quad (14)$$

The kinetic model for the adsorption and desorption reactions yields a Langmuir isotherm for the adsorption behavior of two competitively adsorbed species[37] (see Appendix A).

Assuming that the self-exchange reaction is the fastest of all ET reaction steps and that the rate constants for the self-exchange reaction are similar ($k_{se}^- \approx k_{se}^+$), the ratio θ_{ox}/θ_{red} is defined by the ratio of the redox concentrations at the surface,

$$\theta_{ox}/\theta_{red} \approx c_{ox}^s/c_{red}^s \quad (15)$$

Since the potential of the layer of redox molecules adsorbed at the semiconductor surface is defined by the ratio θ_{ox}/θ_{red} (identical with the ratio of the number of $Co(Cp)_2^+$ and $Co(Cp)_2^0$ molecules), the potential of the layer is determined by the redox potential of the solution if the self-exchange reaction is fast, i.e., significantly faster than the adsorption or desorption reactions (see Appendix A).

For calculating the impedance of this system, it is important to define the quantities that depend on the electrode potential and therefore become time dependent when a small sinusoidal voltage perturbation is superimposed on the electrode potential. The potential-dependent parameters in general are the electron concentration at the semiconductor surface (n_s), the degrees of coverage (θ, θ_{ox}, θ_{red}), the concentrations of the redox couple (c_{ox}^s, c_{red}^s) at the surface if mass transport of the redox species has a limiting influence on the overall charge-transfer process, and the rate constants k_c^- and k_c^+ if a movement of the energy bands at the semiconductor surface occurs. As shown later, the influence of the diffusion of redox ions as well as a movement of the energy bands gain importance if the reduction current exceeds 10% of the diffusion-limited current. However, in this paper we will restrict the impedance analysis to a potential range where band movement has no major influence on the parameters of interest. For this reason we will treat k_c^- and k_c^+ as time-independent constants in the following calculations. Considering now the time-dependent quantities, the complex faradaic ac current ΔI_F follows from eq 12 and is given by eq 16.

$$\Delta I_F = eAN_{ad}^{max}(k_c^+ N_c\,\Delta\theta_{red} - k_c^- n_s \Delta\theta_{ox} - k_c^- \theta_{ox}\Delta n_s) \quad (16)$$

The Δ terms in eq 16 are the complex values of the time-dependent parameters, and the notation as well as the procedure for their evaluation is explained in Appendix B.

The time-dependent variations of the degrees of coverage can be calculated from eq 13. EQCM measurements have shown that the total degree of coverage θ does not change in the potential range of interest, in the depletion region and under current flow. This result suggests that either the rates for the adsorption and desorption reactions are slow compared to the potential changes during the potential scan or the total degree of coverage θ is close to unity. However, with the assumption that $\Delta\theta = 0$, the appropriate rearrangement leads to the relation 17a and b for $\Delta\theta_{ox}$ and $\Delta\theta_{red}$, respectively (it also has to be considered that that $\Delta c_{ox}^s = -\Delta c_{red}^s$).

$$\Delta\theta_{ox} = \frac{[k_{sc}^-\theta_{red} + k_{se}^+\theta_{ox} + k_{ox}^-(1-\theta)]\Delta c_{ox}^s - k_c^-\theta_{ox}\Delta n_s}{i\omega + k_{se}^- c_{ox}^s + k_{se}^+ c_{red}^s + k_c^+ N_c + k_c^- n_s + k_{ox}^+} \quad (17a)$$

$$\Delta\theta_{red} = \frac{-[k_{se}^-\theta_{red} + k_{se}^+\theta_{ox} + k_{red}^+(1-\theta)]\Delta c_{ox}^s + k_c^-\theta_{ox}\Delta n_s}{i\omega + k_{se}^- c_{ox}^s + k_{se}^+ c_{red}^s + k_c^+ N_c + k_c^- n_s + k_{red}^-} \quad (17b)$$

According to the assumption that the $Co(Cp)_2^0$ and $Co(Cp)_2^+$ molecules adsorb competitively at the same kind of adsorption sites, and that $\Delta\theta$ is zero, the time-dependent variations of θ_{ox} must to be equal to the variations of θ_{red}, i.e., $\Delta\theta_{ox} = -\Delta\theta_{red}$. For this reason the terms $k_{ox}^-(1-\theta)$ and $k_{red}^+(1-\theta)$ that describe the adsorption processes have to be negligibly small compared to the other terms in the sum in square brackets in eq 17a and b. This will be the case if either the rate constants k_{ox}^- and k_{red}^+ for the adsorption rates are small or if the total degree of coverage θ is close to unity. If it is further assumed that the rates k_{ox}^+ and k_{red}^- for the desorption processes are negligibly small, the complex time-dependent variations of the degrees of coverage is described by eq 18.

$$\Delta\theta_{ox} = -\Delta\theta_{red} = \frac{(k_{se}^-\theta_{red} + k_{se}^+\theta_{ox})\Delta c_{ox}^s - k_c^-\theta_{ox}\Delta n_s}{i\omega + k_{se}^- c_{ox}^s + k_{se}^+ c_{red}^s + k_c^+ N_c + k_c^- n_s} \tag{18}$$

Equation 18 includes the variation of the surface concentration of the redox couple and the electron density as time-dependent quantities. Consideration of the solution for the variation of the surface redox concentration with the time-dependent faradaic current as given in Appendix C yields eq 19.

$$\Delta\theta_{ox} = -\Delta\theta_{red} = \frac{m_{1,\omega}\dfrac{\Delta I_F}{eAN_{ad}^{max}} - m_2\dfrac{\Delta n_s}{n_s}}{i\omega(1+m_{1,\omega}) + m_3} \tag{19}$$

with

$$m_{1,\omega} = N_{ad}^{max}N_\omega(k_{se}^-\theta_{red} + k_{se}^+\theta_{ox}) \tag{19a}$$

$$m_2 = k_c^- n_s \theta_{ox} \tag{19b}$$

$$m_3 = k_{se}^- c_{ox}^s + k_{se}^+ c_{red}^s + k_c^+ N_c + k_c^- n_s \tag{19c}$$

The time dependence of the faradaic current ΔI_F (eq 16) on a small perturbation voltage ΔU_e that is superimposed on the electrode potential U_e is buried in the time-dependent electron concentration Δn_s at the semiconductor surface. If the electron concentration n_s at the surface is in equilibrium with the electron concentration n_0 in the semiconductor bulk, then according to the Boltzmann relation

$$n_s = n_0 \exp\left[-\frac{e}{kT}\phi_{sc}\right] = n_0 \exp\left[\frac{e}{kT}(U_{fb} - U_e)\right] \quad \text{and} \quad \Delta n_s = -n_s\frac{e}{kT}\Delta U_e \tag{20}$$

where ϕ_{sc} is the potential drop across the space charge layer and U_{fb} is the flatband potential.

The combination of eqs 16, 19, and 20 leads to the faradaic impedance Z_F of the charge-transfer process as defined in eq 21.

$$Z_F = \frac{\Delta U_e}{\Delta I_F} = \frac{kT}{e^2AN_{ad}^{max}}\left[\frac{1 + \dfrac{m_4 m_{1,\omega}}{i\omega(1+m_{1,\omega}) + m_3}}{m_2 - \dfrac{m_4 m_2}{i\omega(1+m_{1,\omega}) + m_3}}\right] \tag{21}$$

with

$$m_4 = k_c^+ N_c + k_c^- n_s \tag{21a}$$

($m_{1,\omega}$, m_2, and m_3 are defined in eq 19a−c)

The frequency characteristics of the faradaic impedance Z_F are identical to the frequency characteristics of the impedance for the equivalent circuit in Figure 6 that is drawn in solid lines. Because of the same frequency dependence, each element of the equivalent circuit in Figure 6 (R_a, R_b, C_b, and Z_w) can be correlated with a kinetic expression that follows from eq 21 through a comparison of the coefficients. The results from the comparison of the coefficients are listed in the following four eqs (22a−d).

$$R_a = \frac{kT}{e^2AN_{ad}^{max}}\left(\frac{1}{k_c^- n_s \theta_{ox}}\right) = R_{ct} \tag{22a}$$

$$R_b = \frac{kT}{e^2AN_{ad}^{max}}\left[\frac{k_c^+ N_c + k_c^- n_s}{k_c^- n_s \theta_{ox}(k_{se}^- c_{ox}^s + k_{se}^+ c_{red}^s)}\right] \tag{22b}$$

$$C_b = \frac{e^2AN_{ad}^{max}}{kT}\left(\frac{k_c^- n_s \theta_{ox}}{k_c^+ N_c + k_c^- n_s}\right) \tag{22c}$$

$$Z_W = N_{ad}^{max}N_\omega(k_{se}^-\theta_{red} + k_{se}^+\theta_{ox})R_b \tag{22d}$$

To derive the total electrochemical impedance at the interface, the nonfaradaic currents ΔI_C must also be taken into account. In general, the capacity of the double-layer capacitance on the electrolyte side of the interface can be assumed to be much larger than the space charge capacitance on the semiconductor side. For this reason, the nonfaradaic current is only due to the charging of the space charge capacitance, i.e., $\Delta I_C = i\omega C_{sc}\Delta U_e$. In an approximation, we assume that the faradaic current is decoupled from the nonfaradaic current.[38] The total current is then the sum $\Delta I_C = \Delta I_F + \Delta I_C$ and the total impedance Z at the semiconductor−electrolyte interface is

$$Z = \frac{1}{\dfrac{1}{Z_F} + i\omega C_{sc}} \tag{23}$$

The impedance of the equivalent circuit that shows the same frequency behavior as the total impedance Z is shown in Figure 6 (solid and dashed lines).[39] Accordingly, this model that invokes a self-exchange reaction would be expected to exhibit an impedance spectrum for a plot in the complex plane that exhibits three features (2 semicircles and 1 asymmetric arc); these are: (1) one semicircle for the charge-transfer reaction between the semiconductor and the adsorbed redox molecules with the time constant $\tau_{ct} = R_aC_{sc} = R_{ct}C_{sc}$, (2) one semicircle for the self-exchange reaction between the adsorbed molecules and the redox molecules in solution with the time constant $\tau_{se} = R_bC_b = (k_{se}^- c_{ox}^s + k_{se}^+ c_{red}^s)^{-1}$, and (3) one asymmetric arc (arc starting with a line of a 45° angle and turning into a semicircle at lower frequencies (usually <1 Hz)) for the diffusion or Warburg impedance Z_w.

As an instructive example, three impedance spectra calculated with different values for the rate constant k_{se} for the self-exchange reaction are shown in Appendix D; a second semicircle in the complex impedance plot develops when $k_{se}^+ = k_{se}^-$ becomes slow.

2. Charge Transfer Taking Thermionic Emission into Account. It has to be considered that the overall charge-transfer event

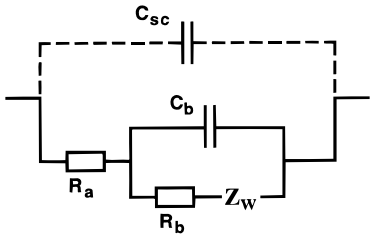

Figure 6. Equivalent circuit that shows the same frequency characteristic for the impedance as the impedance calculated from the kinetic model for charge transfer via a self-exchange reaction (*Z*, eq 23), solid and dashed lines. The faradaic impedance (Z_F, eq 21 and eq 33) for the charge transfer is presented by the circuit in solid lines.

can be limited by the transport of majority charge carriers through the space-charge region if the heterogeneous charge-transfer (eq 8) and the self-exchange reaction (eq 9) are very fast. The overall *measurable* faradic current I_F cannot be higher than the thermionic emission current. The theory according to Bethe assumes that every electron that reaches the semiconductor surface and has the appropriate energy to overcome the potential barrier will cross the interface with a tunnel probability of unity.[40] However, if the kinetics for the heterogeneous charge-transfer reaction is not infinite, some of the charge carriers will be reflected at the interface. As shown in eq 24, the measurable faradaic current I_F will be smaller than the thermionic emission current I_{th} by the fraction *r*.[41]

$$I_F = I_{th}(1 - r) \tag{24}$$

The fraction *r* can vary between 0 and 1. For $r \rightarrow 0$ none of the electrons reaching the interface is reflected; every electron at the semiconductor surface is transferred to an acceptor molecule adsorbed at the semiconductor surface according to the chemical reaction given in eq 8. Since the charge-transfer step is not limiting the current in this case, the kinetic current I_{kin} (defined as the current determined by eq 12) has to be much larger than the measured faradaic current I_F, i.e., $I_{kin} \gg I_F$. In contrast, for $r \rightarrow 1$ nearly every electron reaching the semiconductor surface is reflected. According to the model the electrons are reflected if the charge-transfer reaction (see eq 8) is very slow (e.g., low acceptor concentration or low charge-transfer probability). In this case the kinetic current I_{kin} will become equal to the measured faradaic current I_F, i.e., $I_{kin} \rightarrow I_F$ as $r \rightarrow 1$. Accordingly, the simplest, reasonable expression for the fraction *r* that describes the discussed boundary conditions the proper way is $r \equiv I_F/I_{kin}$. Including the thermionic emission, the measurable, stationary faradaic current is now

$$\frac{1}{I_F} = \frac{1}{I_{th}} + \frac{1}{I_{kin}} \tag{25}$$

and the time-dependent measurable faradaic current is

$$\Delta I_F = I_F^2\left(\frac{\Delta I_{th}}{I_{th}^2} + \frac{\Delta I_{kin}}{I_{kin}^2}\right) \tag{26}$$

It should be noted that for all expressions in this section (eqs 25−34), the various relationships between the dependent and independent variables and parameters differ from those in the previous section (eqs 12−23) because eqs 25−34 include the effects of thermionic emission in the model. Equations 12−23 are only valid for the case where the rate of thermionic emission is always faster than the rate of electron transfer.

The back reaction, that is the electron injection from the adsorbed molecules into the conduction band of the n-type semiconductor, is already defined in the kinetic expression 12 and has to be the same for the thermionic emission current. Since both currents (I_{kin} and I_{th}) contain the same kinetic expression for the back reaction, a clear separation of both reaction paths will be difficult. For the sake of simplicity, we assume a perfect rectifying behavior of the semiconductor electrode in the following considerations and neglect the anodic current. With this, the thermionic current can be written as

$$I_{th} = -AA^*\left(\frac{m^*}{m_e}\right)T^2\left(\frac{n_s}{n_0}\right)\exp\left[-\frac{1}{nkT}(E_F - E_c)\right] \tag{27}$$

and

$$\Delta I_{th} = I_{th}\frac{\Delta n_s}{n_s} \tag{28}$$

(The introduction of the carrier concentrations n_0 and n_s into the thermionic emission current assumes the applicability of eq 20. Restrictions are discussed later in this section.)

In eq 27, A^* is the Richardson constant (120 A K^{-1} cm^{-2}), m^*/m_e is the relative effective electron mass in the conduction band, *T* is the temperature, and *n* is the quality factor. For the sake of simplicity, the quality factor is considered to be 1 in the following theoretical considerations.

The time-dependent kinetic current is

$$\Delta I_{kin} = -eAN_{ad}^{max}k_c^-(\theta_{ox}\Delta n_s + n_s\Delta\theta_{ox}) = I_{kin}\frac{\Delta n_s}{n_s} + I_{kin}\frac{\Delta\theta_{ox}}{\theta_{ox}} \tag{29}$$

Inserting eqs 28 and 29 into eq 26 yields eq 30 for the time-dependent measurable faradaic current

$$\Delta I_F = I_F\frac{\Delta n_s}{n_s} + \frac{I_F^2}{I_{kin}}\frac{\Delta\theta_{ox}}{\theta_{ox}} \tag{30}$$

For the calculation of the time-dependent degree of coverage from eq 13b, it has to be taken into account that reaction rate R_c^- for the heterogeneous electron transfer is now defined by eq 31.

$$R_c^- = -\frac{I_F}{eA} = -\frac{1}{eA}\left(\frac{I_{th}I_{kin}}{I_{th} + I_{kin}}\right) \tag{31}$$

The combination of eq 13b (with $R_c^+ \approx 0$, $R_{ox}^- = 0$ and $R_{ox}^+ = 0$), eq 31, and eq C4 (Appendix C) yields for the time-dependent degree of coverage eq 32.

$$\Delta\theta_{ox} = -\Delta\theta_{red} = \frac{m_{1,\omega}\dfrac{\Delta I_F}{eAN_{ad}^{max}} - m_2'\dfrac{\Delta n}{n_s}}{i\omega(1 + m_{1,\omega}) + m_3'} \tag{32}$$

with

$$m_2' = -\frac{I_F}{eAN_{ad}^{max}} \tag{32a}$$

$$m_3' = k_{se}^- c_{ox}^s + k_{se}^+ c_{red}^s + \left(\frac{I_F}{I_{kin}}\right)^2 k_c^- n_s \tag{32b}$$

($m_{1,\omega}$: see eq 19a)

For the calculation of the faradaic impedance it has to be assumed that the Fermi level is constant from the interior of the semiconductor to the surface. This will be approximately the case if the diffusion of the electrons is very fast.[40] Then, the electron concentration n_s at the surface can be calculated from the Boltzmann relation (eq 20). As it will be shown later in the discussion of the experimental results, a net current flow across the interface does not significantly alter the concentration profile that is found under equilibrium conditions. This conclusion follows from the fact that the I−V (and R−V) characteristics of the n-GaAs electrodes still show a linear behavior in a semilogarithmic plot with a slope of approximately 60 mV per decade. This ideal behavior is not expected if the diffusion perturbs the Fermi level at the surface. For this reason, eq 20 is also assumed to be valid even for currents in the order of the thermionic emission current. The calculation of the faradaic impedance from the combination of eqs 30, 32, and 20 yields eq 33.

$$Z_F = \frac{\Delta U_e}{\Delta I_F} = \frac{kT}{e^2 AN_{ad}^{max}} \left[\frac{1 + \dfrac{m_4' m_{1,\omega}}{i\omega(1 + m_{1,\omega}) + m_3'}}{m_2' - \dfrac{m_4' m_2'}{i\omega(1 + m_{1,\omega}) + m_3'}} \right] \tag{33}$$

with

$$m_4' = -\frac{I_F}{eAN_{ad}^{max}} \frac{I_F}{I_{kin}\theta_{ox}} = \left(\frac{I_F}{I_{kin}}\right)^2 k_c^- n_s \tag{33a}$$

($m_{1,\omega}$: see eq 19a. m_2': see eq 32a. m_3': see eq 32b.)

The faradaic impedance Z_F of eq 33 shows the same frequency dependence as the faradaic impedance Z_F of eq 21 or the equivalent circuit displayed in Figure 6 (solid and dashed lines). However, the comparison of the coefficients yields for the elements R_a, R_b, C_b, and Z_W a different set of kinetic expressions, which are listed in eq 34a−d.

$$R_a = \frac{kT}{e}\frac{1}{-I_F} = \frac{kT}{e}\left(\frac{1}{-I_{th}} + \frac{1}{-I_{kin}}\right) = R_{th} + R_{ct} \tag{34a}$$

$$R_b = \frac{kT}{e^2 AN_{ad}^{max}} \left[\frac{\left(\dfrac{I_F}{I_{kin}}\right)^2 k_c^- n_s}{\dfrac{-I_F}{eAN_{ad}^{max}}(k_{se}^- c_{ox}^s + k_{se}^+ c_{red}^s)} \right] \tag{34b}$$

$$C_b = \frac{e^2 AN_{ad}^{max}}{kT} \left[\frac{\dfrac{-I_F}{eAN_{ad}^{max}}}{\left(\dfrac{I_F}{I_{kin}}\right)^2 k_c^- n_s} \right] \tag{34c}$$

$$Z_W = N_{ad}^{max} N_\omega (k_{se}^- \theta_{red} + k_{se}^+ \theta_{ox}) R_b \tag{34d}$$

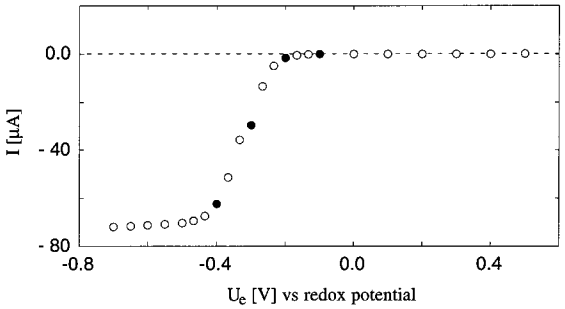

Figure 7. Stationary current−potential curve for the $Co(Cp)_2^+$ reduction at an n-GaAs RDE (200 rpm) in ACN−$TBAPF_6$ (0.3 M). Other parameters are $[Co(Cp)_2^+] = 1.3$ mM and $[Co(Cp)_2^0] = 0.9$ mM, and the electrode area is 0.152 cm^2. For the four potentials marked with filled circles the EIS are shown in Figure 8.

The time constant τ_{ct} [$\tau_{ct} = R_a C_{sc} = (R_{ct} + R_{th})C_{sc}$] is here defined by the space charge capacitance and the sum of the resistance R_{ct} for the heterogeneous charge transfer and the resistance R_{th} for the thermionic emission. A single impedance measurement does not allow one to distinguish whether the charge transfer is limited by thermionic emission or the charge-transfer step. But according to eq 34a, the resistance R_a will only show a dependence on the degree of coverage θ_{ox} or θ_{red} and subsequently a concentration dependence if the charge transfer is limited by the heterogeneous charge-transfer reaction and not by thermionic emission. The time constant τ_{se} [$\tau_{se} = R_b C_b = (k_{se}^- c_{ox}^s + k_{se}^+ c_{red}^s)^{-1}$] for the self-exchange reaction is not affected by the current limitation through thermionic emission, as expected. The expression 34d for the Warburg impedance Z_W is identical with eq 22d although the correct term for the resistance R_b has to be considered for the calculations.

B. Results And Discussion of Impedance Data. Figure 7 shows an I−V curve for a stationary current−voltage measurement for $Co(Cp)_2^+$ reduction ($[Co(Cp)_2^+] = 1.3$ mM, $[Co(Cp)_2^0] = 0.9$ mM) at an n-GaAs RDE in ACN-$TBAPF_6$ (0.3 M) at 200 rpm. The measurement covers the potential range of the depletion region (+0.5 V to −0.1 V), the current onset region (from −0.1 V to −0.2 V), the region of sharp current rise (from −0.2 V to −0.4 V), and the diffusion-limited region (from −0.4 V to −0.7 V). The diffusion-limited current here amounts to 71 μA. For each I−V-data point, the frequency dependence of the impedance was recorded between 1 Hz and 600 kHz. For the four black marked I−V data points in Figure 7, the EIS are shown as a plot in the complex impedance plane in Figure 8a−d. In the current onset region at −0.1 V and −0.2 V (Figure 8a and b), where the faradaic current is small compared to the diffusion-limited current, the EIS show one single semicircle. The EIS recorded at −0.3 V and −0.4 V (Figure 8c and d) in the current rise region, where the faradaic currents exceed 10% of the diffusion-limited current, show as an additional feature in the spectra, the Warburg impedance (Z_W), that is due to the diffusion of the redox species.

The dashed lines in Figure 8 are the best fits according to the equivalent circuit in Figure 6 assuming that the self-exchange rate is infinitely fast, i.e., the resistance R_b approaches such small values that the time constant τ_{se} cannot be resolved. None of the EIS that were recorded for the $Co(Cp)_2^+$ reduction at GaAs revealed a third time constant that would indicate that the adsorption of redox molecules is an important reaction step in the charge-transfer mechanism. This lack of a third relaxation time in the EIS led us to the previous assumption that no other more complicated mechanism than a simple second-order reaction was involved in the total charge-transfer reaction.[2]

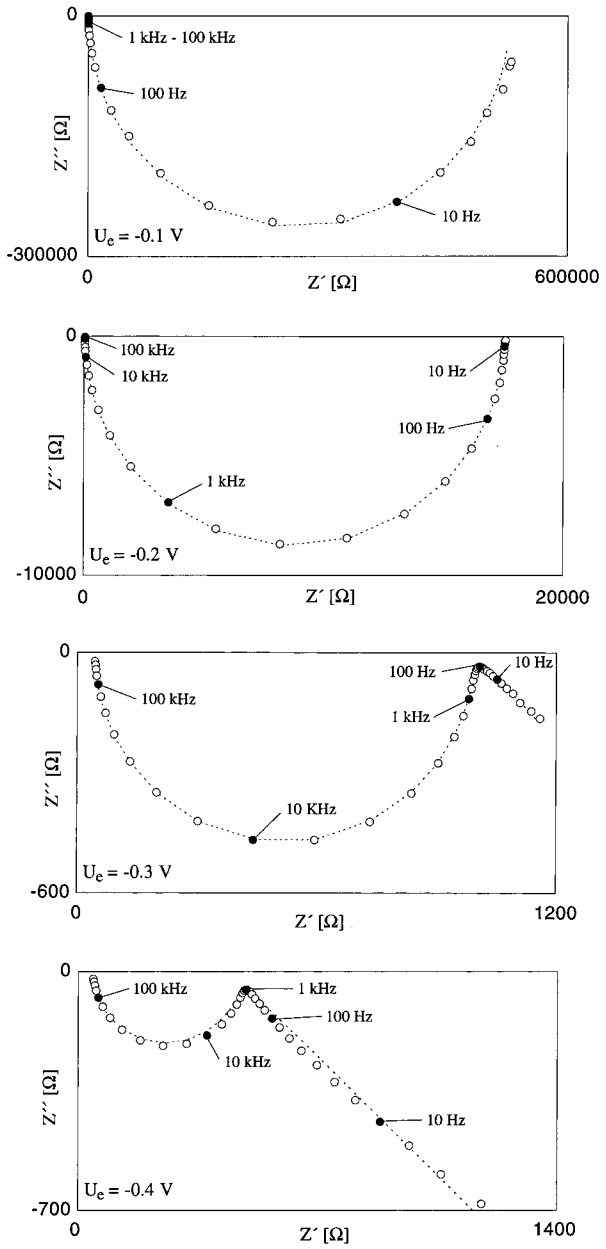

Figure 8. Four EIS recorded at (a) −0.1 V, (b) −0.2 V, (c) −0.3 V, and (d) −0.4 V (see Figure 7 for corresponding I−V data). The EIS are shown in the complex plane in the frequency range between 1 Hz to 600 kHz. The dashed lines show the best fit according to the model assuming a very fast self-exchange reaction with $k_{se} > 10^{-14}$ cm^3 s^{-1}. For other parameters see caption of Figure 7.

The rate constant for the homogeneous self-exchange reaction between $Co(Cp)_2^+$ and $Co(Cp)_2^0$ redox molecules in ACN amounts to $k_{se} = 7 \times 10^{-14}$ cm^3 s^{-1} as reported in the literature.[42−44] Assuming that the adsorption of the redox molecules does not have a drastic impact on the rate constant for the homogeneous self-exchange reaction, the value of $k_{se} = 7 \times 10^{-14}$ cm^3 s^{-1} can be used to calculate the relaxation time using eq 22b and c. This calculation yields $\tau_{se} \approx 10^{-5}$ s ([$Co(Cp)_2^+$] = 1.3 mM, [$Co(Cp)_2^0$] = 0.9 mM; $k_{se}^- = k_{se}^+$); thus, the frequency marking the semicircle top is expected to be 16 kHz. As seen from the impedance spectra in the current step region (Figure 8c and d), τ_{se} is very similar to the time constant τ_{ct} which makes a resolution of both charge-transfer steps impossible. The equation for the self-exchange resistor R_b (eq 22b) allows for an estimation of whether the relaxation time τ_{se} or τ_{ct} dominates in the region of current flow. Compared to

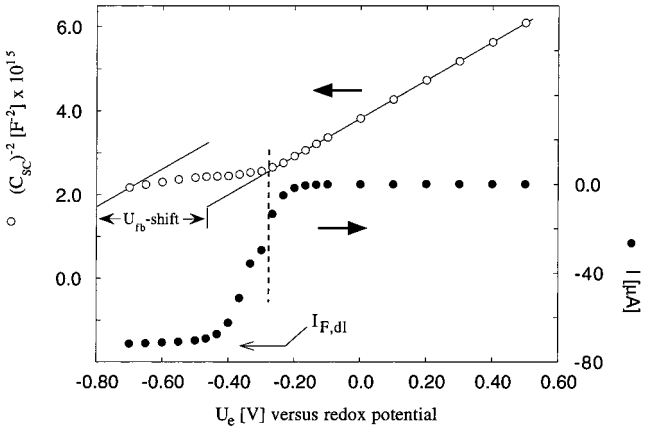

Figure 9. Mott−Schottky plot of the capacitance versus the electrode potential (upper part, left scale) as evaluated from the semicircles of the EIS. Comparison with the current−potential data (lower part, right scale) reveals that the energy bands shift to negative potentials when the faradaic current exceeds 10% of the diffusion-limited current.

$k_c^- n_s$ the term $k_c^+ N_c$ becomes negligibly small in the current onset region, and the resistor R_b becomes independent of the quantities k_c^-, k_c^+, and n_s. Using the experimental values for the quantities of interest ($A = 0.152$ cm^2, $\theta_{ox} = 0.59$ (for $\theta = 1$), and $N_{ad}^{max} = 4 \times 10^{14}$ cm^{-2}) the resistor R_b is calculated to be smaller than 0.05 Ω. A semicircle with a diameter of 0.05 Ω is far too small to be resolved in the EIS shown in Figure 8. The tendency of the shape of the impedance spectra for increasing values of the rate constant k_{se} is shown in Figure 15 (Appendix D). According to the simulations, k_{se} must be smaller than 10^{-15} cm^3 s^{-1} to resolve the relaxation time for the self-exchange reaction in the EIS. Therefore, the semicircle in the EIS of Figures 8a to 8d has to be attributed to the relaxation time $\tau_{ct} = R_{ct}C_{sc}$ for the heterogeneous charge transfer between electrons in the GaAs conduction band and the adsorbed $Co(Cp)_2^{+/0}$ molecules.

The capacitance values as calculated from the semicircles of the EIS are plotted in the Mott−Schottky manner ($1/C^2$ vs U_e) in the upper part of Figure 9 (left scale). The data points fit very well on a straight line in the depletion region. According to the Mott−Schottky theory the linear part of the plot yields information about the doping density N_d and the flatband potential U_{fb} (see eq 35).

$$\frac{1}{C_{sc}} = \frac{2}{e\epsilon\epsilon_0 N_d A^2}\left(\phi_{sc} - \frac{kT}{e}\right) \qquad \text{with}$$

$$\phi_{sc} = -(U_{fb} - U_e) \quad (35)$$

where ϵ is the relative dielectric constant, ϵ_0 is the permittivity of free space, and N_d is the doping density.

The value for the doping density calculated from the slope of the linear region matches well with the value determined from Hall measurements. This confirms that the measured capacitance is the space charge capacitance of the n-GaAs electrode.

A comparison of the Mott−Schottky data with the current−voltage data, which are plotted in the lower part of Figure 9 (right scale), reveals that the Mott−Schottky data fit well on the straight line only if the faradaic currents do not exceed 10% of the diffusion-limited current. This indicates that no band movement, and hence no surface state charging, occurs at the GaAs−electrolyte interface in the current onset region. However, for faradaic currents higher than 10% of the diffusion-limited current (see vertical dashed line in Figure 9), the flatband

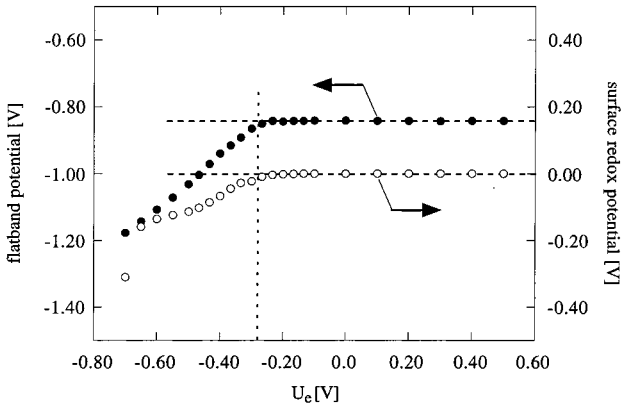

Figure 10. Comparison of the flatband potential (calculated from the Mott−Schottky plot) with the surface redox potential (calculated from the diffusion-limited current using eq 36) as a function of electrode potential. The flatband potential and hence the energy bands at the surface shift negative at the same potential where the surface redox potential starts to move to negative potentials, i.e., when the faradaic current exceeds 10% of the diffusion-limited current (see vertical dashed line).

potential (and hence the position of the energy bands) starts to move toward negative potentials. The flatband potential shift increases with negative bias into the diffusion-limited current region. This "unpinning" of the energy bands in the region of the current rise provides evidence that the charge-transfer reaction in this region does not follow a simple model with fixed band edges and a second-order rate law.[2]

A more detailed evaluation of the flatband potential shift in the current step is presented in Figure 10. Here, the flatband potential shift and the surface redox potential are plotted versus the electrode potential. The surface redox potential was calculated using eq 36 which is derived from the Nernst relation[37] and eq 37 (considering that c_{ox}^{s} is zero in the diffusion-limited region).

$$U_{redox}^{s} = U_{redox}^{0} + \frac{kT}{e}\ln\left\{\frac{1-\frac{I_F}{I_{F,dl}}}{\exp\left[\frac{e}{kT}(U_{redox}^{0}-U_{redox}^{b})\right]+\frac{I_F}{I_{F,dl}}}\right\} \quad (36)$$

where U_{redox}^{s} is the surface redox potential, U_{redox}^{0} is the standard redox potential, U_{redox}^{b} is the redox potential in solution bulk, and $I_{F,dl}$ is the diffusion-limited faradaic current, and

$$I_F = eA\left(\frac{D_{ox}}{\delta_{N,ox}}\right)(c_{ox}^{s}-c_{ox}^{b}) = eA\left(\frac{D_{red}}{\delta_{N,red}}\right)(c_{red}^{b}-c_{red}^{s}) \quad (37)$$

where A is electrode area, D_{ox} or D_{red} are the diffusion coefficients of the redox species, c_{ox} or c_{red} are the concentrations of the redox species, and $\delta_{N,ox}$ or $\delta_{N,red}$ are the thicknesses of the Nernst diffusion layers.

In Figure 10 the flatband potential shift in the current rise and the diffusion-limited current region was calculated for each Mott−Schottky data point with the reasonable assumption that the slope of the Mott−Schottky line does not change. The graph shows that the energy bands at the GaAs−electrolyte interface start to move when the redox potential at the electrode surface shifts to negative potentials due to the influence of diffusion limitation of the redox species at the electrode surface (see vertical dashed line in Figure 10).[45] This simultaneous shift of

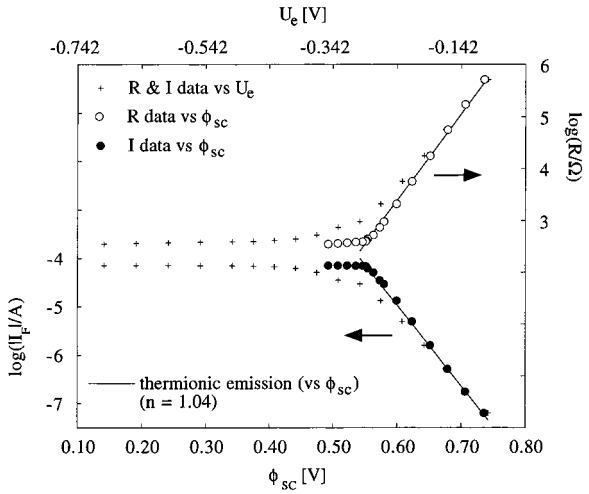

Figure 11. Faradaic current and resistance R_a, as obtained from the semicircles of the EIS, plotted versus the electrode potential (cross marked data points, upper *x*-scale) and the band bending in the GaAs electrode (circles, lower *x*-scale). The solid lines are calculated according to the thermionic emission theory.

the surface redox potential and the flatband potential indicates that a strong coupling exists between the GaAs electrode and the redox couple molecules. Such an "unpinning" of the energy bands occurs if the redox species interacts more strongly with the GaAs surface than with the solvent molecules.[46] Because the concentration of the redox molecules ($[Co(Cp)_2^{+/0}] \approx 10^{-3}$ M) is 4 orders of magnitude smaller than the concentration of the solvent molecules ([ACN] ≈ 19 M), it is likely that the redox molecules have to be adsorbed at the semiconductor surface to cause an unpinning of the energy bands. The unpinning of the energy bands (Fermi-level pinning) at the n-GaAs−ACN interface through $Co(Cp)_2^{+/0}$ has been reported in the literature at various times,[47−50] but to our knowledge it has never been reported to be caused by adsorption of the $Co(Cp)_2^{+/0}$ molecules at the GaAs surface.

In our model, the potential barrier at the semiconductor-electrolyte interface is defined by the adsorbed layer of redox molecules. Therefore, an equal shift of the flatband and the surface redox potential is expected if the potential barrier does not change in the considered potential range.

Knowledge of the flatband potential U_{fb} allows one to calculate the bending of the energy bands ϕ_{sc} at each electrode potential U_e (according to eq 35). In Figure 11 the resistance as obtained from the EIS (open circles, upper part, right scale) and the faradaic current (full circles, lower part, left scale) are plotted versus the band bending ϕ_{sc} (bottom *x*-axis scale). In this figure, the R_a and I_F data points marked as crosses are also plotted versus the electrode potential U_e (*x*-axis scale on top), i.e., assuming that the energy bands do not move and that the flatband potential remains constant at $U_{fb} = -0.842$ V as determined from the Mott−Schottky plot in the depletion region. Without considering the band movement, only the data points at high band bendings and low faradaic currents show a slope of approximately 60 mV per I_F or R_a decade, as theoretically expected. However, if the band movement is taken into account (according to $\phi_{sc} = -(\delta U_{fb} + U_{fb} - U_e)$), then nearly all I_F and R_a data points (filled and open circles) exhibit a potential dependence of 60 mV per I_F or R_a decade, as theoretically expected. A potential dependence of 60 mV per decade is other unequivocal evidence that the semicircle in the EIS of Figure 8 is due to the relaxation time $\tau_{ct} = R_{ct}C_{sc}$ for the heterogeneous charge-transfer reaction.

We further assume that the potential barrier for the majority charge carriers at the n-GaAs−$Co(Cp)_2^{+/0}$(ad) interface does not change within the current step. According to the model, a constant potential barrier means that the shift of the flatband potential and the potential of the adsorbed layer of redox molecules is identical and equal to the shift of the surface redox potential. The coincidental shift of the flatband potential and the surface redox potential has been (qualitatively) shown in Figure 10.

The calculation of the rate constant k_c^- from the I_F and R_a vs ϕ_{sc} plot according to eqs 12 and 22a, respectively, yields $k_c^- = 1.2 \times 10^{-7}$ cm^3 s^{-1}. This value can only be exactly assigned to k_c^- if the charge transfer between the n-GaAs and the adsorbed $Co(Cp)_2^{+/0}$ molecules is the rate-limiting step in the overall charge-transfer reaction; otherwise, it is a lower limit. However, it will be shown in the following paragraph that the thermionic emission of majority charge carriers is limiting the current rather than the electrochemical charge-transfer reaction. Our previous published results[2] on the concentration dependence of the current−voltage characteristics of the n-GaAs/$Co(Cp)_2^{+/0}$ system also indicates that the rate of thermionic emission limits the observed faradaic current when the concentration of the $Co(Cp)_2^+$ acceptor is sufficiently high. In that study, the current was found to depend approximately linearly on the $Co(Cp)_2^+$ concentration only when it was between 0.27 and 1.9 mM; at higher concentrations the current started to become independent of $Co(Cp)_2^+$ concentration and saturated at 17 mM. Thus, while in the previous study thermionic emission began to limit the current above 1.9 mM, we show below that in the present study thermionic limitation of the current is present at 1.3 mM $Co(Cp)_2^+$. We attribute the somewhat lower value of $Co(Cp)_2^+$ concentration at which thermionic emission is rate limiting to the higher [$Co(Cp)_2^0$/$Co(Cp)_2^+$] ratio in the present experiments; because of the Nernst relationship, the higher ratio produces a more negative redox potential for the solution, a smaller band bending, a greater surface electron concentration, and hence faster ET rates for given electrode potentials.

The solid lines in Figure 11 have been calculated according to the thermionic emission theory (using an ideality factor of $n = 1.04$); the justification of n is discussed in ref 2, assuming that the transport of majority charge carriers in the space charge layer of the semiconductor is limiting the overall charge-transfer process. Both the I_F and R_a data points fit very well on the solid line, which supports the assumption that thermionic emission is the current-limiting transport mechanism. As explained in more detail in the theory part of this section (IV.A.2.), the overall current cannot be higher than the thermionic current. But since the thermionic emission current is limiting the charge transfer, the rate constant k_c^- for the kinetic current has to be larger than 1.2×10^{-7} cm^3 s^{-1} according to eqs 25 and 34a for the faradaic current I_F and the resistance R_a, respectively.

To confirm that the faradaic current at negative potentials (from −0.4 V to −0.7 V in Figure 7) is indeed limited by the diffusion of the redox active species, the limited current was recorded at different rotation velocities. According to the Levich theory for rotating disk electrodes, the plot of the diffusion-limited current versus the square root of the angular velocity yields a straight line that crosses the origin (eq 38).[37]

$$I_{F,dl} = eA\left(\frac{D_{ox}}{\delta_{N,ox}}\right)c_{ox}$$

with

$$\delta_{N,ox} = 1.61\, \nu^{1/6} D_{ox}^{1/3} \omega^{-1/2} \tag{38}$$

where $I_{F,dl}$ is the diffusion-limited current, ν is the kinematic viscosity, and ω is the angular velocity.

Figure 12 shows the dependence of the limited current for the $Co(Cp)_2^+$ reduction in ACN on the rotation velocity of the n-GaAs−RDE between 50 and 1200 rpm. The Levich plot in Figure 12a fits very well on a straight line that crosses the origin. With $c_{ox} = 1.5$ mM, $A = 0.152$ cm^2, and $\nu = 5.8 \times 10^{-3}$ cm^2 s^{-1},[51] the diffusion coefficient for the $Co(Cp)_2^+$ ion, as calculated from the slope, amounts to $D_{ox} = 1.3 \times 10^{-5}$ cm^2 s^{-1}. This value is in good agreement with the value for the diffusion coefficient obtained from similar studies at metal−RDE (platinum, gold).

Figure 12b shows a plot of the reciprocal of the limited current versus the reciprocal of the square-root of the angular frequency. For this type of plot a finite intercept is expected if any processes other than the diffusion of the active redox species becomes the limiting mechanism for the overall current (e.g., diffusion at partially blocked electrodes,[52−54] or preceding heterogeneous (adsorption) or homogeneous chemical (dissociation) reactions[37]). However, the linear fit in Figure 12b does not show an intercept within the range of error, and therefore the limited current for the $Co(Cp)_2^+$ reduction at n-GaAs is considered to be the diffusion-limited current.

The observation of the theoretically expected rotation dependence of the diffusion-limited current allows an estimation of a lower value for the rate constant k_{se}, i.e., a lowest value, which provides a minimum current flow, such that the self-exchange reaction does not show a significant limiting influence on the overall charge transfer. The rotation-speed-dependent quantities are the gradients of the redox concentrations at the electrode according to eq 37 and subsequently the degrees of coverage θ_{ox} and θ_{red}. For this estimation it is sufficient just to consider θ_{ox}. θ_{ox} is rewritten in the form of eq 39 that follows from eq 13b with $I_F = eA(\times c2_c + - \times c2_c^-)$, $\times c2_{ox}^+ = \times c2_{ox}^- = 0$ and $k_{se} = k_{se}^- = k_{se}^+$.

$$\theta_{ox} = \frac{k_{se} c_{ox}^s \theta + \dfrac{I_F}{eAN_{ad}^{max}}}{k_{se}(c_{ox}^s + c_{red}^s)} \tag{39}$$

The surface concentrations (c_{ox}^s, c_{red}^s) in eq 39 are replaced by the appropriate term of eq 37. With the assumption that $D = D_{ox} = D_{red}$ and $\delta_N = \delta_{N,ox} = \delta_{N,red}$, the rearrangement of eq 39 leads to

$$\theta_{ox} = \frac{k_{se}\left(\dfrac{I_F}{eA}\dfrac{\delta_N}{D}\right)\theta + \dfrac{I_F}{eAN_{ad}^{max}}}{k_{se}(c_{ox}^b + c_{red}^b)} \tag{40}$$

and

$$\theta_{ox} = \left(\frac{c_{ox}^b \theta}{c_{ox}^b + c_{red}^b}\right) + \frac{\left(N_{ad}^{max} k_{se} \theta \dfrac{\delta_N}{D} + 1\right)}{k_{se}(c_{ox}^b + c_{red}^b)} \frac{I_F}{eAN_{ad}^{max}} \tag{41}$$

The rotation speed dependence of θ_{ox} is buried in δ_N (see eq 38) and according to eq 41 is only expected if

$$N_{ad}^{max} k_{se} \theta \frac{\delta_N}{D} > 1 \tag{42}$$

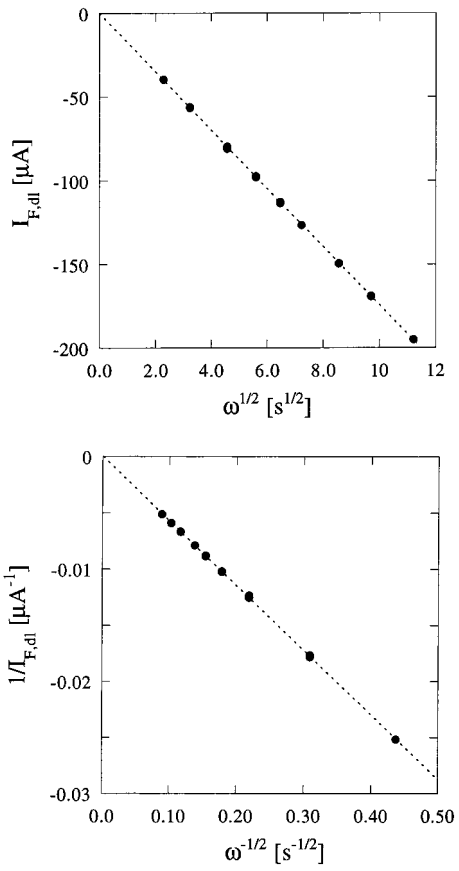

Figure 12. (a) Levich plot of the diffusion-limited currents (I_{dl}) recorded for the $Co(Cp)_2^+$ reduction at n-GaAs at different rotation speeds between 50 and 1200 rpm ($\omega = 2\pi f$). The electrode area was 0.152 cm^2, and the $Co(Cp)_2^+$ concentration was 1.5 mM. (b) Plot of the reciprocal of the diffusion-limited current ($1/I_{dl}$) versus the reciprocal of the square root of the angular velocity ($1/\sqrt{\omega}$).

regardless of the current-limiting transport mechanism. That is, for $N_{ad}^{max} = 4 \times 10^{14}$ cm^{-2}, $\theta = 1$, $\delta_N = 1.43 \times 10^{-3}$ cm (for 1200 rpm), and $D = 1.3 \times 10^{-5}$ cm^2 s^{-1}, the rate constant k_{se} for the self-exchange reaction has to be at least larger than 3×10^{-17} cm^3 s^{-1}. This result is qualitatively in agreement with the results from the EIS measurements where we concluded that k_{se} is larger than 10^{-14} cm^3 s^{-1}. However, it has to be noted that the EIS analysis is in general more sensitive than the electrochemical analysis of the diffusion-limited current. Therefore it is reasonable to assume that the rate constant k_{se} for the self-exchange reaction is in the order of 10^{-14} cm^3 s^{-1}.

In conclusion, the electrochemical studies of the reduction of $Co(Cp)_2^+$ at n-GaAs electrodes in ACN show that both charge-transfer steps, namely, the heterogeneous charge transfer from the n-GaAs electrode to the adsorbed $Co(Cp)_2^{+/0}$ molecules and the self-exchange charge transfer from the adsorbed $Co(Cp)_2^{+/0}$ molecules to the $Co(Cp)_2^{+/0}$ molecules in solution are considered to be fast. The rate constant k_{se} for the self-exchange reaction has to be larger than 10^{-14} cm^3 s^{-1} (concluded from the fact that the EIS only exhibit two relaxation times) and since the overall current is limited by thermionic emission, the rate constant k_c- for the heterogeneous charge transfer must be larger than 1.2×10^{-7} cm^3 s^{-1}. Consequences of these results for the dynamics of ET will be discussed below in section VI.

V. Theory of the GaAs/$Co(Cp)_2^{+/0}$ Interface

Since new rigorous theoretical approaches to the description of the SMI have been recently developed,[55,56] these types of calculations were applied to the GaAs/$Co(Cp)_2^{+/0}$/ACN system to determine whether the model proposed here, which involves adsorption of the $Co(Cp)_2^{+/0}$ redox system onto the GaAs surface, and the corresponding experimental results are consistent with theoretical expectations. This is necessary because metallocenes, such as $Co(Cp)_2^{+/0}$, have previously been generally presumed to be nonadsorbing, outersphere types of redox molecules at SMIs.[6,8,10,27,28]

A. Theoretical Methods. Our goal is to calculate the adsorption energetics and molecular configuration of $Co(Cp)_2^+$ and $Co(Cp)_2^0$ on GaAs surfaces with the redox molecules dissolved in ACN. Calculations of adsorption energies and molecular configurations for semiconductor−vacuum interfaces are very challenging primarily because electron correlation and exchange must be accurately addressed; the SMI with liquid present is even more challenging primarily because near-surface solvent molecule orientation, adsorbed solvent, and adsorbed oxygen affect the adsorption of the redox species. Notwithstanding, we show below that adsorption energies and geometries can be calculated for the SMI system of interest in this paper.

For adsorption at vacuum interfaces, density functional theory (DFT) methods have been used predominantly. The latest DFT methods use nonlocal pseudopotentials[57−61] (including generalized gradient (GGA) functionals) and some methods also include HF exchange. The error in the calculated adsorption energies, relative to experiment for systems explored thus far, is typically in the range of 0.1−0.5 eV. We have adopted a cluster calculation approach to the adsorption problem at liquid interfaces, which is described below. We found the $Co(Cp)_2^{+/0}$/GaAs system extremely computationally demanding at the DFT BLYP (Becke−Lee−Yang−Par) and B3LYP level (B3LYP is one of the most accurate DFT methods) when used with the high-level quantum-chemistry basis sets implemented in the PS-GVB program.[62] Thus, our combined requirements of accuracy and computational tractability necessitated that we employ an assortment of methods to address adsorption for the $Co(Cp)_2^{+/0}$. These methods are

Full B3LYP. Full B3LYP calculations were performed on small clusters.

B3LYP−PSCF. In this method we first performed with PS-GVB, full ab initio Hartree−Fock (with the high-level basis set denoted as LACVP**) calculations on larger clusters.[62] We then evaluated the LACVP** HF post SCF wave functions via the high-level DFT method (B3LYP) provided in the PS-GVB program suite. This post self-consistent field (PSCF) method represents an approximation to the full B3LYP method; other PSCF methods are possible within PS-GVB.

CI. CI calculations were also performed on small systems.

R−PM3. Small cluster B3LYP and larger scale B3LYP−PSCF results were fit to the PM3 Hamiltonian of MOPAC by a method described below. The reparametrized PM3 (R−PM3) method was subsequently used on very large systems.

First Principles Molecular Dynamics. We also performed preliminary first principles MD simulations, of the same kind we have done for another system,[56] using the R−PM3 electronic structure method to calculate the interatomic forces for the fully solvated $Co(Cp)_2^{+/0}$/GaAs/ACN system. We also addressed solvation with higher level methods as discussed below.

Regarding the R−PM3 method, we chose standard PM3 parameters for all elements in the GaAs/$CO(Cp)_2^{+/0}$/ACN system except Co. Since we have not yet completed our own s-, p-, and d-orbital-based PM3 program, we chose a PM3 s- and p-orbital model for cobalt. We denote our model R−PM3 metallocene as $M(Cp)_2^{+/0}$. We then varied PM3 parameters for

M to fit $Co(Cp)_2^{+/0}$/GaAs results obtained from full B3LYP, LACVP**, and B3LYP−PSCF calculations for adsorbate geometry, binding energy, and other energetics. The orbital structure of the cobalt complex is obviously only roughly characterized without true d-orbitals. But for present purposes we are most interested in fitting B3LYP energetics and geometry, and our results indicate the R−PM3 approach is able to reproduce these features qualitatively. The PM3 parameters ultimately chosen for M, are closest to PM3 Ga. The optimized geometry of $Ga(Cp)_2^{+/0}$, using even essentially standard PM3 Ga, is remarkably similar to that for $Co(Cp)_2^{+/0}$, and the match to B3LYP adsorption energy profiles as a function of distance is similar. This R−PM3 electronic structure method was useful for qualitative adsorption geometry and energetics and also to explore the effects of very large semiconductor and ACN clusters which would be computationally prohibitive with the other methods. Further progress along these lines must await completion of our d-orbital PM3 code.

The GaAs (100) surface in UHV conditions undergoes a number of reconstructions, as has been analyzed in detail both experimentally and theoretically.[61,63−65] It is computationally prohibitive for us to let the surface reconstruct self-consistently via BLYP methods to examine the effect of the solvent on the reconstruction. Thus, in our calculations we simply chose two representative surface structures. One of these is the (2 × 1) dimer UHV reconstruction, while the other is cleanly terminated (100) GaAs. We examine both As and Ga-terminated surfaces. Our cleanly terminated surface has the main characteristics of the UHV (100) GaAs reconstructions (e.g., all Ga or As on the surface), but the arrangement of the atoms on the surface is not of the proper reconstructed geometry, and this can have profound effects.

Other complications of our system include oxidation of the GaAs surface and solvent adsorption. We do not include oxide layers in the calculations, but we do address solvent (ACN) adsorption (it is found to be weaker than $Co(Cp)_2^{+/0}$ adsorption).

B. Results. We find below that the adsorption energy for all methods employed is less than 1.0 eV both for $Co(Cp)_2^+$ and $Co(Cp)_2^0$, and for both the reconstructed (2 × 1) dimer[65] ((2 × 1) D) and cleanly terminated (CT), hydrogen-passivated (100) GaAs surfaces. In these cases there is so little charge exchange with the surface, and small enough polarization, that the cobalt complexes essentially maintain their gas-phase geometry (the rings themselves can freely rotate). Only in the case where one of the CT surface Ga atoms was left unpassivated by hydrogen, did the geometry of adsorbed $Co(Cp)_2^{+/0}$ significantly distort. In light of these results, we take a conservative viewpoint and use only the (2 × 1) D or fully hydrogen-passivated CT (100) GaAs surface in the discussions below.

With the two types of surfaces described above, we performed adsorption calculations both for a UHV system (no solvent, only GaAs and $Co(Cp)_2^{+/0}$) and the solvated system (GaAs/$Co(Cp)_2^{+/0}$/ACN).

We calculated the minimum energy adsorption configuration at the B3LYP−PSCF level for the UHV system using an 18-atom GaAs(100) CT cluster. For this case, upright (end on) and parallel face configurations were examined. A much larger UHV geometry optimization search was performed with MOPAC's BFGS method using our R−PM3 with a large 50-atom CT cluster. The lowest energy configuration for the solvated system was determined with our R−PM3 first-principles MD simulation.

The preferred adsorption geometry, in both the UHV and solvated case, appears to be with the rings of $Co(Cp)_2^{+/0}$ parallel to the surface (Figure 13). For the (2 × 1) D surface two of the carbons of the cyclopentadienyl (Cp) ring prefer to be close to a Ga dimer of the Ga-terminated (2 × 1) D surface, as shown in Figure 13b. The As-terminated (2 × 1) D surface undergoes less electron density exchange with the $Co(Cp)_2^{+/0}$ than the Ga termination, and the adsorption is weak enough that the minimum energy surface site is not clear, but the preferred geometry is still parallel. In the parallel geometry the adsorption primarily involves π-system interaction of the Cp groups with the GaAs. For the CT surface the adsorption energy is roughly the same as for the 2 × 1 D and with the parallel geometry preferred. There is some artifactual binding of the complex with the passivating hydrogen atoms in the CT case. Ideally the H atoms should be indifferent spectator atoms only serving to passivate dangling bonds. The dipole resulting from H−Ga or H−As bonds is different than the Ga−As dipole and can significantly affect the adsorption energy of the charged cobaltocenium. While these geometries seem to minimize the energy, a thorough test was simply computationally prohibitive with the higher level methods. Thus our adsorption energy estimates reported below with the high level methods are, again, lower bounds. The adsorption could be stronger for different redox species/GaAs substrate geometries.

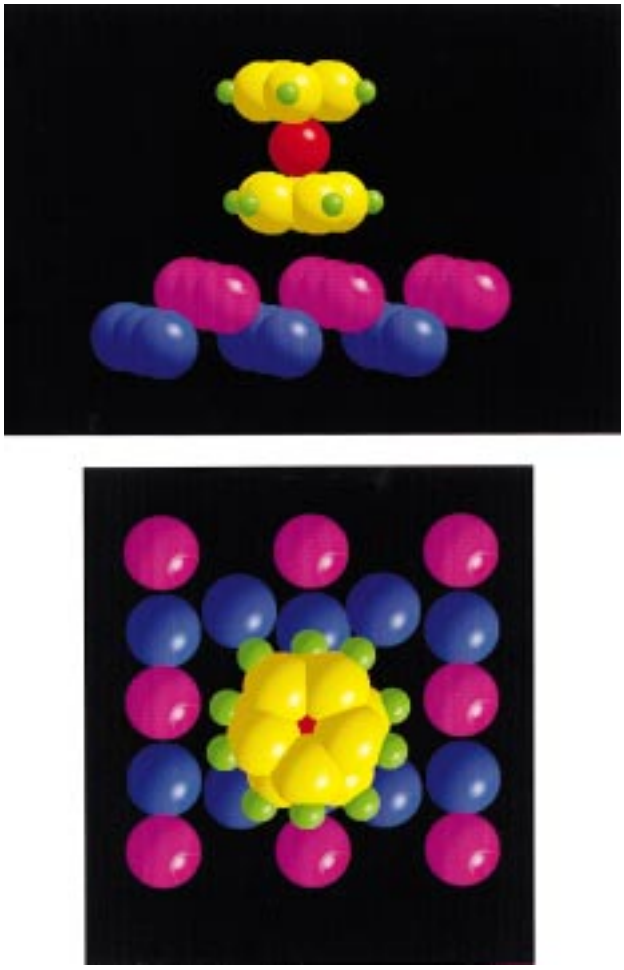

Figure 13. Orientation and geometry of $Co(Cp)_2^+$ adsorbed on (100) GaAs: (a) side view looking along the cleanly terminated (100) GaAs surface with Ga termination and full hydrogen passivation (H atoms not shown) and (b) top view looking down on reconstructed (2 × 1) dimer (100) GaAs surface. Cyclopentadienyl rings are parallel to the GaAs surface.

The adsorption energy for $Co(Cp)_2^{+/0}$ on (2 × 1) D and CT 100 GaAs is of order 1.0 eV or less for all theoretical methods applied to both the oxidized and reduced cobalt species, and in

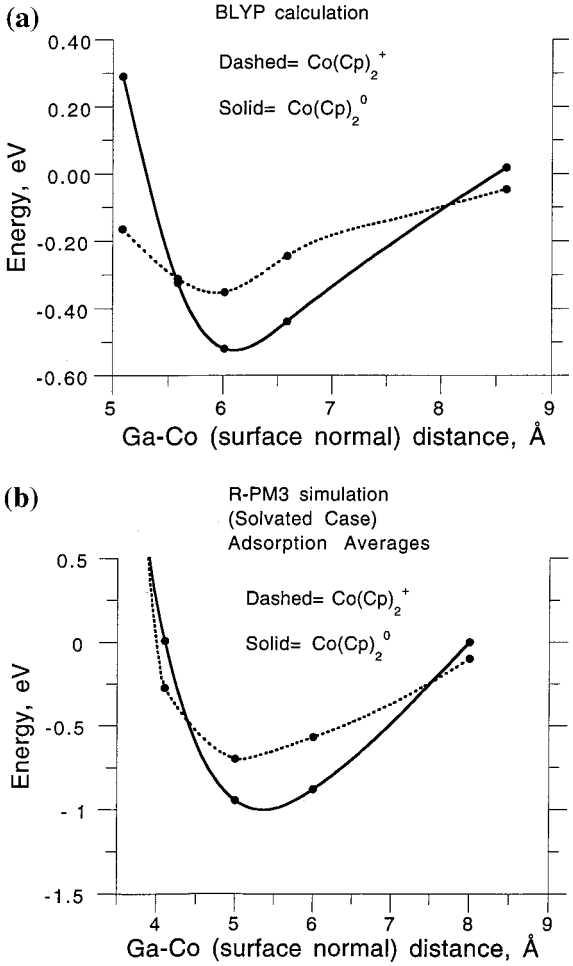

Figure 14. Energy vs Ga−Co distance for $Co(Cp)_2^+$ at cleanly terminated (100) GaAs with Ga termination: (a) BLYP calculation and (b) R−PM2 simulation (the energies are averages over time).

both the UHV and solvated cases. Our calculations in Figures 14a and 14b show that the adsorption energy seems somewhat greater for the cobaltocene species than cobaltocenium both in the UHV and solvated cases. But with such a complicated interface, the error in the calculations could easily be judged to be a few tenths of an eV, which is about equal to the maximum estimated difference in the adsorption energy. The BLYP calculations are, of course, the most accurate. These adsorption energy values (about 0.55 and 0.35 eV, for cobaltocene and cobaltocenium respectively, see Figure 14a), are in reasonable agreement with the experimental results (solvation does not significantly affect the average adsorption energy, as discussed further below). However, all DFT methods such as B3LYP are expected to underestimate the actual adsorption energy since the calculated correlation energy is usually too small. The actual surface may also be significantly different than the theoretical ones. The most important point is that high level theory (BLYP) does predict that metallocenes can, indeed, adsorb on the (100) GaAs surface. Note that the adsorption energy of the lowest level method employed (R−PM3) is about twice that of the B3LYP calculations (Figure 13a), but the qualitative trends are the same, and the quantitative trends are similar. While the R−PM3 method was fit to the BLYP methods by varying the model Co parameters, it is difficult to offset our R−PM3's apparent tendency to overestimate the adsorption energy.

Figure 14b shows the results of a R−PM3 first-principles MD simulation for the average adsorption energy in the solvated system as a function of distance from the surface. About 200 solvent molecules were used. Near-surface solvent was treated quantum mechanically (via R− PM3), while the remaining solvent was addressed with conventional classical MD methods. This hybrid approach was implemented in exactly the same fashion as in ref 56. All semiconductor atoms were treated quantum mechanically. The polarization of the surface by the ACN and the polarization of and by the $Co(Cp)_2^{0/+}$ both affect the adsorption energy. The *average* adsorption energy in the solvated R−PM3 system relative to the R−PM3 UHV adsorption energy is, remarkably, not dramatically affected by the presence of the solvent. This kind of phenomenon has been seen in other solid−liquid-interface adsorption studies.[66] In our case this appears to be primarily a result of the absence of solvent molecules between the semiconductor and the redox species and the fact that dipolar and charge exchange interactions mutually perpendicular to the surface and the $Co(Cp)_2^{+/0}$ rings (rather than lateral interactions) are most important in the adsorption. This is also consistent with our high level UHV calculations.

In summary, the maximum adsorption energy occurs with both $Co(Cp)_2^+$ and $Co(Cp)_2^0$ having their cyclopentadienyl rings parallel to the GaAs surface, rather than edge on, and in all cases the calculated adsorption energy is of order 1.0 eV or less. The possibility that $Co(Cp)_2^{+/0}$ dissociates on the (100) GaAs surface is remote based on our calculations. The rings are rather strongly bound, and our calculated electron density exchange is rather small.

C. Possible Adsorption-Mediated ET Scenarios. On the basis of our experimental and calculated adsorption energies, we assume both cobalt complexes are adsorbed, and a steady-state coverage is formed on the surface; thus, the primary role played by the adsorbed species is mediating the ET to redox species in solution. The latter species may also adsorb onto the previously established $Co(Cp)_2^{+/0}$ layer, and with the face parallel geometry it is possible that stacking of $Co(Cp)_2^{+/0}$ could occur. However, our EQCM results indicate that stacking (i.e., multilayer formation) does not occur If an adsorbed monolayer does not act as a favorable substrate for further cobalt species adsorption, then we effectively have a modified electrode surface that can mediate ET to cobalt species near the surface.

Another possibility is that an irreversibly adsorbed layer could form a cobalt metal−semiconductor interface (Schottky junction). Our experiments do not support this possibility, and our calculations also indicate that it is unlikely either cobalt redox species dissociates.

When both redox species adsorb, there are a number of possible ET scenarios. Since the $Co(Cp)_2^+$ is positively charged and its charge exchange on adsorption to the semiconductor is calculated to be relatively small, it could form a long-range Coulombic trap for electrons. If a solvated $Co(Cp)_2^+$ in solution approaches the adsorbed and reduced $Co(Cp)_2^+$ (i.e., $Co(Cp)_2^0$), then the latter species could transfer the transiently trapped electron to the former species. In other words, the adsorbed cobalt species could form a spatially local density of states, i.e., a surface-localized density of states (surface state) that could transfer charge to acceptors in solution. This is similar to homogeneous ET between the $Co(Cp)_2^{+/0}$ species in solution, but in this case coupling to semiconductor eigenstates can have profound effects on the ET, and reorganizational modes can also be dramatically affected. The trapped electron would have a lifetime determined primarily by the strength of the electronic interaction of the orbital (in which it is trapped) to the semiconductor (roughly, lifetime $= \hbar/|v|$, where $|v|$ is the electronic coupling matrix element).

Adsorbed (neutral) $Co(Cp)_2^0$ could also trap electrons for a sufficient period of time to pass them to a neighboring $Co(Cp)_2^+$ in solution. As is well-known from UHV studies, quasistationary states of this kind can have lifetimes over the femtosecond-to-nanosecond range. In UHV studies on metal electrodes it is thought that the exit of the electron from the neutral back into the metal can sometimes induce desorption. Here the trapped state would dissipate some of its probability density into the redox species, and some into the semiconductor.

VI. Concluding Discussion

Traditional models for ET from semiconductors to redox molecules in solution[1,3,10,67,68] assume nonadsorbing outersphere redox species;[3,10] the metallocenes and their cations were generally believed to fall into this class of redox molecules.[6,8,10,27,28]

However, the results reported here show that adsorption of the $Co(Cp)_2^{+/0}$ metallocene redox system occurs on GaAs and those adsorptions plays a critical role in the dynamics of ET. The adsorption energies are found to be relatively small (experimentally, about 0.2 and 0.4 eV for $Co(Cp)_2^+$ and $Co(Cp)_2^0$, respectively), and therefore the adsorption type is closer to physisorption than chemisorption. The electronic coupling matrix element ($|\upsilon|$) between $Co(Cp)_2^+$ and GaAs has been estimated to be about 0.01 eV.[69] This magnitude of coupling is much too high to safely classify the ET as nonadiabatic, and it is too low to be categorically described as adiabatic. It is best categorized as an intermediate regime. It should be realized that the electronic coupling can change significantly with configuration of the redox species relative to the surface (especially with respect to surface site location), and with surface reconstruction and contamination. Thus, the actual value for the experimental system could deviate from the calculated value by a significant factor. Simple models indicate full electronic adiabaticity might be achieved with a $|\upsilon|$ as low as 0.03 eV.

The ultralarge second-order heterogeneous rate constants (k_{ET} 1×10^{-10} cm^4/s) reported previously for ET across the GaAs/$Co(Cp)_2^{+/0}$ interface[2] were calculated assuming bulk solution concentrations of $Co(Cp)_2^+$, i.e., adsorption was not considered. From the present analysis of our impedance and current−potential data based on the model in Figure 5, we estimate the minimum heterogeneous rate constant for ET from GaAs to adsorbed $Co(Cp)_2^+$ to be $k_c^- = 1.2 \times 10^{-7}$cm^3/s. The units of k_c^- are cm^3/s because the concentration of adsorbed acceptors is expressed as an areal density. If one takes the thickness of the layer containing the adsorbed $Co(Cp)_2^+$ to be 8 Å (the sum of the molecule thickness and the distance from the surface at which the adsorption energy was calculated to be a maximum (see Figure 14), then the effective value of the second-order rate constant using volumetric units for the acceptor is $k_{ET} = (1.2 \times 10^{-7})(8 \times 10^{-8}) \cong 1 \times 10^{-14}$ cm^4/s.

Since the electron coupling between $Co(Cp)_2^+$ and GaAs is believed to be relatively small (estimated to be 0.01 eV) and the acceptor is weakly adsorbed, the k_{ET} value (1×10^{-14} cm^4/s) can be roughly compared to the value of 1×10^{-17} cm^4/s, which has been proposed as the upper limit for ET to nonadsorbed, ideal outersphere acceptors.[4−10] Our k_{ET} value estimated here is about 3 orders of magnitude larger than the supposed upper limit and is more consistent with upper-limit values reported by Smith et al.[26,56] Thus, the discrepancy between our reported k_{ET} values and the upper limit values predicted in refs 9 and 10 is reduced from about 6 orders of magnitude (reported in ref 2) to about 3 orders of magnitude as adsorption is taken into account.[70] The remaining discrepancy of about 3 orders of magnitude can be attributed both to the degree to which the GaAs/$Co(Cp)_2^+$ system falls outside the limits of conventional outersphere ET and deficiencies of the model of refs 9 and 10.

The second-order rate constants for the GaAs/$Co(Cp)_2^+$ system can be converted into an electron-transfer velocity (S_{ET}, cm/s) or into a cross section (σ_{ET}, cm^2) using the following simple relationships:

$$S_{ET} = k_{ET}c_{ox} = k_c^- N_{ad}^{ox} \approx 5 \times 10^6 \text{ cm/s}$$

and

$$\sigma_{ET} = S_{ET}/\upsilon_{th}N_{ad}^{ox} = k_c^-/\upsilon_{th} = 1.2 \times 10^{-14} \text{ cm}^2$$

where υ_{th} is the thermal velocity of electrons (1×10^7 cm/s) and N_{ad}^{ox} is the areal density of acceptors.

Both of these numbers indicate ultrafast ET dynamics. The electron-transfer velocity is comparable to the highest values of the recombination velocity reported for electrons for nonradiative recombination dynamics at surface states and/or adsorbed species on semiconductor surfaces.[71,72] Within experimental error, the cross section is in the range of the physical area of the $Co(Cp)_2^+$ acceptor molecule. A simple-minded conversion of S_{ET} into a photoinduced electron-transfer time (obtained by dividing S_{ET} into the absorption depth) yields a few ps. However, the actual physical significance of the electron-transfer velocity, the cross section, and the electron-transfer time is more complicated than that implied by the simple interpretation implied above, and a deeper theoretical analysis is required for the interpretation of these numbers.[69]

It is of interest to compare the values of the ET rate constants that we report here for GaAs/$Co(Cp)_2^+$ to related III−V semiconductor−metallocene−metallocenium systems in the literature.[1,3,13,4−10] In all these previous experiments the metallocenium electron acceptors or metallocene hole acceptors were assumed to be nonadsorbed to the semiconductor surface. In ref 8, experiments based on dark I−V and Mott−Schottky plots reported an upper limit for k_{ET} for the n-GaAs/ACN/Fe$(Cp)_2^+$ system to be $<1 \times 10^{-14}$ cm^4/s; for p-InP/CH_3OH/Co$(Cp)_2^+$ the upper limit for the rate constant for hole transfer was reported to be $<1 \times 10^{-13}$ cm^4/s. For n-InP in methanol with $Fe(Cp)_2^+$ and several substituted ferrocenium acceptors,[6] k_{ET} was reported to be 1×10^{-16} to 10^{-17} cm^4/s.

Rate constants for photoinduced ET from p-type GaAs and InP electrodes with metallocenium acceptors in ACN have also been reported based on PL quenching experiments.[1,13] In these experiments it was again assumed that the metallocenium acceptors are not adsorbed. For p-GaAs sulfided with Na_2S to reduce intrinsic surface recombination, the reported k_{ET} value was 4×10^{-13} cm^4/s for $Co(Cp)_2^+$ and 2×10^{-12} cm^4/s for $Fe(Cp)_2^+$; S_{ET} was 4×10^4 and 2×10^5 cm/s for 0.5 mM solutions, respectively.[13] A recent reexamination of these data (Poles, E.; Smith, B.; Nozik, A. J. Unpublished results.) using a Monte-Carlo model yields S_{ET} and k_{ET} values of about 7×10^3 cm/s and 1×10^{-14} cm^4/s, respectively, for $Co(Cp)_2^+$ (1.0 mM) and 10^4 cm/s and $\sim 4 \times 10^{-14}$ cm^4/s for $Fe(Cp)_2^+$ (0.5 mM), respectively. In a very recent study[1] using pristine GaAs surfaces with $Fe(Cp)_2^+$, S_{ET} was reported to be 7×10^3 cm/s for 10 mM $Fe(Cp)_2^+$, and the cross section was 2×10^{-15} cm^2 (compared to our estimate of 1.2×10^{-14} cm^2); these values lead to a k_{ET} of 2×10^{-15} cm^4/s. Again, no enhancement of acceptor concentration by adsorption was believed to occur, and it was estimated that the S_{ET} value would increase to 1×10^7

cm/s if a full monolayer of adsorbed $Fe(Cp)_2^+$ was formed on the GaAs surface.[1]

A major outstanding issue for the comparison of the various reported values of S_{ET}, k_{ET}, and cross section is whether the acceptor is adsorbed or not. Our QCM experiments show that in the case of our etched epilayer GaAs electrodes, physisorption of both $Co(Cp)_2^+$ and $Co(Cp)_2$ occurs; $Co(Cp)_2^+$ was also found to adsorb to quartz and gold surfaces, but did not absorb onto nylon surfaces. Our preliminary QCM experiments with $Fe(Cp)_2^+$ indicates that this molecule is also adsorbed to GaAs. Thus, if adsorption is present in the experiments of refs 1 and 13, then the calculated k_{ET} could be reduced by several orders of magnitude depending upon the acceptor concentration and adsorption isotherm. We note that since in ref 1 the projected value of S_{ET} for a full adsorbed monolayer of $Co(Cp)_2^+$ is 1×10^7 cm/s, which is consistent with what we find here with the known adsorption of $Co(Cp)_2^+$, this suggests that the $Co(Cp)_2^+$ is not adsorbed in that specific experimental system. The factors controlling whether acceptors are adsorbed or not on III−V surfaces are not understood, but this factor will make very large differences in the rates of ET and the calculated rate constants. Determination of adsorption in any given system will require an independent measurement using, for example, QCM, IR reflection spectroscopy, or SHG.

Concerning the issue of hot electron transfer across semiconductor surfaces, what matters here is the net rate of ET, not the rate constant; that is, the *rate* of ET has to be faster than the *rate* of hot electron cooling (reported hot electron cooling times range from several hundred fs to several hundred ps). In refs 4 and 10, the analysis of ET kinetics led to the reported upper limit for k_{ET} of about 1×10^{17} cm^4/s (and also assuming nonadsorption of acceptors); this then led to the conclusion that hot electron transfer is not possible with nonadsorbed acceptors.[10] This is because with a maximum k_{ET} of 1×10^{-17} cm^4/s and an acceptor concentration of say 100 mM, S_{ET} would only be $(1 \times 10^{-17}\ \text{cm}^4/\text{s}) \times (6 \times 10^{19}\ \text{cm}^{-3}) = 600$ cm/s, and the ET time would be roughly $(\alpha S_{ET})^{-1} \sim 50$ ns, not fast enough to compete with hot electron cooling. However, as we show here, adsorption of so-called outersphere acceptors, such as metallocenes and their cations does occur, and this can increase the ET rate or S_{ET} by 3−5 orders of magnitude compared to the case where there is no adsorption; thus, in the case of adsorbed acceptors, the ET rate can be 500 fs to 50 ps, which is competitive with hot electron cooling. Furthermore, as seen in the present experiment, the ET process can be mediated through the adsorbed molecules (i.e., through a self- exchange ET reaction between adsorbed $Co(Cp)_2^{+/0}$ and free $Co(Cp)_2^+$ in solution), preventing the buildup of more than one monolayer of reactant and product and allowing for ultrafast steady-state ET and current flow.

Acknowledgment. This work was supported by the U.S. Department of Energy, Office of Science, Office of Basic Energy Sciences, Division of Chemical Sciences. K.S. was supported by the Deutsche Forschungsgemeinschaft and supervised at ISFH by R. Memming and R. Reineke-Koch. We thank Mark C. Hanna for providing the epilayer GaAs samples, A. Duda for advice on sample preparation for QCM measurements, and R.J.D. Miller for useful comments.

Appendix A

The Langmuir isotherm follows from eq 13 if only the mass balance is considered (i.e., none of the charge-transfer events is admitted). For stationary conditions ($d\theta/dt = d\theta_{ox}/dt = d\theta_{red}/dt = 0$), eqs 13b, 13c, and 14 yield

$$\theta_{ox}\beta_{ox}(1-\theta)c_{ox}^s \tag{A1}$$

$$\theta_{red} = \beta_{red}(1-\theta)c_{red}^s \tag{A2}$$

$$\frac{\theta}{(1-\theta)} = \beta_{ox}c_{ox}^s = \beta_{red}c_{red}^s \tag{A3}$$

with $\beta_{ox} = k_{ox}^-/k_{ox}^+$ and $\beta_{red} = k_{red}^+/k_{red}^-$. The β-term can be identified with the definition given in eq 5. The adsorption strength of each species in this kinetic evaluation is expressed through the ratio of rate constants for the adsorption and desorption reactions.

The combination of the balance eqs 13b, 13c, and 14 gives the relations A4 and A5 for the dependence of the degrees of coverage θ_{ox} and θ_{red} on the rate constants, the electron density at the surface, and the concentration of the redox species.

$$\theta_{ox} = \frac{(k_{se}^-c_{ox}^s + k_c^+N_c)\theta + k_{ox}^-c_{ox}^3(1-\theta)}{k_{se}^-c_{ox}^s + k_{se}^+c_{red}^s + k_c^+N_c + k_c^-n_s + k_{ox}^+} \tag{A4}$$

$$\theta_{red} = \frac{(k_{se}^+c_{red}^s + k_c^-n_s)\theta + k_{red}^+c_{red}^s(1-\theta)}{k_{se}^-c_{ox}^s + k_{se}^+c_{red}^s + k_c^+N_c + k_c^-n_s + k_{red}^-} \tag{A5}$$

Relations A4 and A5 allow a discussion about the state of occupation as defined by the ratio of the degrees of coverage θ_{ox}/θ_{red}. The ratio θ_{ox}/θ_{red} at a given ratio of the redox concentrations depends on the chemical reactions as defined in eqs 8 to 11. Assuming first that no charge transfer occurs via the adsorbed layer ($k_c+ = k_c- = 0$) and that the self-exchange reaction is negligibly slow ($k_{se}^+c_{red}^s$, $k_{se}^-c_{ox}^s \ll k_{red}^-$, k_{ox}^+), i.e., only adsorption and desorption reactions take place, then the ratio θ_{ox}/θ_{red} is given by

$$\frac{\theta_{ox}}{\theta_{red}} = \frac{\beta_{ox}}{\beta_{red}}\frac{c_{ox}^s}{c_{red}^s} \tag{A6}$$

According to eq A6, the ratio θ_{ox}/θ_{red} depends strongly on the ratio β_{ox}/β_{red} that takes the difference of the adsorption energies into account. If charge transfer is allowed and assuming that the charge exchange via the adsorbed layer of redox molecules is the fastest of all ET reaction steps, whereas adsorption and desorption reactions are negligibly slow (k_{red}^-, k_{ox}^+, k_{red}^+, $k_{ox}^- \rightarrow 0$), then the ratio θ_{ox}/θ_{red} is defined through

$$\frac{\theta_{ox}}{\theta_{red}} \rightarrow \frac{k_{se}^-}{k_{se}^+}\frac{c_{ox}^s}{c_{red}^s} \tag{A7}$$

Appendix B

In this publication the complex notation is used to calculate the impedance of the electrochemical system. The purpose of Appendix B is to impart the basics of this mathematical treatment to the reader to understand the derivations. A more detailed treatise is given in text books.[73,74]

For the measurement of the impedance the dc voltage Ü applied to a system is superimposed by a sinusoidal ac perturbation voltage U_t (frequency, $\nu = \omega/(2\pi)$; phase angle, ϕ_U, amplitude $\hat{U}$). The mathematical treatment using the Euler identity is shown in eq B1.

$$U = \ddot{U} + U_t = \ddot{U} + \hat{U}\exp[i(\phi_U + \omega t)] = \ddot{U} + \Delta U \exp(i\omega t) \quad \text{(B1)}$$

with

$$\Delta U = \hat{U}\exp[i\phi_U]$$

(i is the imaginary number, $i = (-1)^{1/2}$; ω is the angular frequency of the voltage perturbation, and t is the time)

The current response of the system is modulated with the same frequency and can be separated into a dc current part $\ddot{I}$ and into an ac current part $\hat{I}$ as shown in eq B2.

$$I = \ddot{I} + I_t = \ddot{I} + \hat{I}\exp[i(\phi_I + \omega t)] = \ddot{I} + \Delta I \exp(i\omega t) \quad \text{(B2)}$$

with

$$\Delta I = \hat{I}\exp[i\phi_I]$$

According to the definition, the impedance of the system is defined through the ratio of the complex quantities ΔU and ΔI. If the Euler identity is used, the impedance can be separated into a complex number as shown in eq B3.

$$Z = \frac{\Delta U}{\Delta I} = \frac{\hat{U}}{\hat{I}}\exp[i(\phi_U - \phi_I)] = \frac{\hat{U}}{\hat{I}}\cos(\phi_U - \phi_I) + i\frac{\hat{U}}{\hat{I}}\sin(\phi_U - \phi_I) \quad \text{(B3)}$$

In eq B3 the impedance is the sum of the real part Z' (cos term) and the 90° phase-shifted imaginary part Z'' (sin term).

$$Z = Z' + iZ'' \quad \text{(B4)}$$

Most of the electrochemical systems are nonlinear, but if the perturbation signal (voltage) is kept sufficiently small ($\Delta U < e/(kT) \approx 25$ mV), the variation of the quantity of interest can be calculated from a Taylor series that is developed around the stationary value and truncated after the second term. This linearization procedure is shown in eq B5 for the faradaic current I_F.

$$I_F = \ddot{I}_F + \left(\frac{dI_F}{dU}\right)\Delta U \exp(i\omega t) \quad \text{(B5)}$$

and with consideration of eq B2

$$\Delta I_F = \left(\frac{dI_F}{dU}\right)\Delta U \quad \text{(B6)}$$

The capacitive charging currents I_C are expressed as time-dependent voltage variations across a capacitance C, i.e., $I_C = (dU/dt)C$. Considering that the time-independent dc currents do not show any contribution, the linearization procedure yields

$$\Delta I_C \exp(i\omega t) = C\frac{d}{dt}[\Delta U \exp(i\omega t)] \quad \text{(B7)}$$

and

$$\Delta I_C = i\omega C \Delta U \quad \text{(B8)}$$

Appendix C

Appendix C shows a solution for the calculation of the complex, time-dependent variations of the surface concentration due to a time-dependent perturbation of the electrode potential if the electrode surface is covered with a layer of adsorbed redox molecules. For this calculation we define the number of molecules that are exactly at the electrode surface but not adsorbed as N_{redox} (the unit of N_{redox} is molecules × cm^{-2}). The time-dependent changes of N_{redox} can be expressed in terms of the self-exchange rate:[75]

$$\nu_{ox} = -\nu_{red} \equiv \frac{dN_{ox}}{dt} = -\frac{dN_{red}}{dt} = R_{se}^{+} - R_{se}^{-} \quad \text{(C1)}$$

Assuming that the self-exchange reaction is much faster than the adsorption and desorption reaction, the rate ν_{ox} equals the difference between the flux of charge carriers through the interface (i.e., $I_F/(eA) = \times c2_c^{+} - \times c2_c^{-}$) and the time-dependent changes of the coverage of adsorbed acceptor molecules (i.e., $N_{ad}^{max}\, d\theta_{ox}/dt \approx \times c2_{se}^{-} - \times c2_{se}^{+} + \times c2_c^{+} - \times c2_c^{-}$). An analogous relation for ν_{red} follows:

$$\frac{\nu_{ox}}{N_{ad}^{max}} = -\frac{\nu_{red}}{N_{ad}^{max}} = \frac{I_F}{eAN_{ad}^{max}} - \frac{d\theta_{ox}}{dt} = \frac{I_F}{eAN_{ad}^{max}} + \frac{d\theta_{red}}{dt} \quad \text{(C2)}$$

Keeping in mind that $d(\theta + \Delta\theta\exp[i\omega t])/dt = i\omega\Delta\theta\exp[i\omega t]$, the variations of the rates ν_{ox} and ν_{red} are

$$\frac{\Delta\nu_{ox}}{N_{ad}^{max}} = -\frac{\Delta\nu_{red}}{N_{ad}^{max}} = \frac{\Delta I_F}{eAN_{ad}^{max}} - i\omega\Delta\theta_{ox} = \frac{\Delta I_F}{eAN_{ad}^{max}} + i\omega\Delta\theta_{red} \quad \text{(C3)}$$

The variation of the rate has to be coupled with the diffusion equations; the boundary conditions of the laatter problem are defined by the experimental setup. For a rotating disk electrode, the solution is[74−76]

$$\Delta\nu_{redox} = \frac{1}{N_{\omega,redox}}\Delta c_{redox}^{s} \qquad \text{with} \qquad N_{\omega,redox} = \frac{\tanh\left(\delta_{N,redox}\sqrt{\frac{i\omega}{D_{redox}}}\right)}{\sqrt{i\omega D_{redox}}} \quad \text{(C4)}$$

which holds either for the reduced or oxidized species if the diffusion coefficients or thicknesses of the Nernst diffusion layers are different (i.e., $D_{ox} \neq D_{red}$ and $\delta_{N,ox} \neq \delta_{N,red}$). However, assuming that $D_{ox} = D_{red}$ and $\delta_{N,ox} = \delta_{N,red}$, the combination of eqs C3 and C4 yields the relationship between the time-dependent variations of the degrees of coverage, the faradaic current, and the surface concentration of the redox system as shown in eq C5.

$$\Delta c_{ox}^{s} = -\Delta c_{red}^{s} = -N_{ad}^{max}N_{\omega}\left(i\omega\Delta\theta_{ox} - \frac{\Delta I_F}{eAN_{ad}^{max}}\right) = N_{ad}^{max}N_{\omega}\left(i\omega\Delta\theta_{red} + \frac{\Delta I_F}{eAN_{ad}^{max}}\right) \quad \text{(C5)}$$

Appendix D

Figure 15 shows the experimental impedance spectra (M, open circles) of Figure 8c recorded at −0.3 V vs solution redox potential and three simulated impedance spectra (S(1) to S(3), lines with black dots) calculated for different rate constants k_{se} for the self-exchange reaction. The values of k_{se} used for the simulations are listed in Table 1. Table 1 also contains the calculated values for the faradaic current I_F, the degrees of coverage θ_{ox} and θ_{red}, the time constant $\tau_{ct} = R_aC_{sc}$, and the

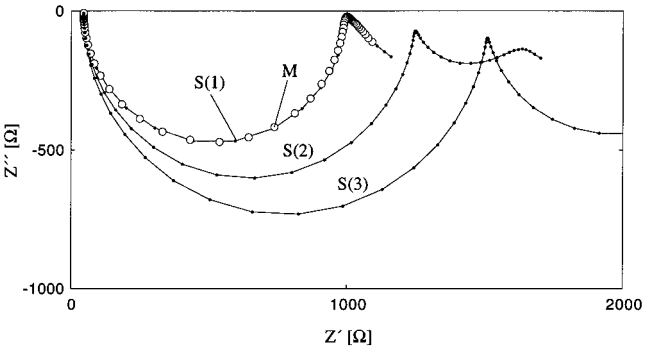

Figure 15. Experimental EIS (M, open circles, recorded at −0.3 V) and three simulated impedance spectra (S(1) to S(3), lines with black dots) calculated for different rate constants k_{se} for the self-exchange reaction (see Table 1).

TABLE 1: Faradaic Current (I_F) Degrees of Coverage (θ_{ox}/θ_{red}), and the Relaxation Times for the Heterogeneous Charge Transfer and the Self-Exchange Reaction (τ_{ct} and τ_{se}) Calculated for Three Different Rate Constants for the Self-Exchange Reaction

curve	$k_{se}^+ = k_{se}^-$ [cm^3 s^{-1}]	I_F [A]	θ_{ox}/θ_{red}	τ_{ct} [s]	τ_{se} [s]
S1	$<1.0 \times 10^{-14}$	-2.7×10^{-5}	0.59/0.41	1.9×10^{-5}	7.6×10^{-5}
S2	1.0×10^{-16}	-2.1×10^{-5}	0.46/0.54	2.4×10^{-5}	7.6×10^{-3}
S3	5.0×10^{-17}	-1.7×10^{-5}	0.38/0.62	3.0×10^{-5}	1.5×10^{-2}

time constant $\tau_{se} = R_b C_b$. The spectra were calculated for a frequency range from 1 Hz to 1 MHz.

Other parameters are the following: $\phi_{sc} = 0.542$ V ($+U_e = -0.3$ V); $N_d = 1.0 \times 10^{17}$ cm^{-3}; $A = 0.152$ cm^2; $c_{ox} = 1.3$ mM; $c_{red} = 0.9$ mM; $D = 1.3 \times 10^{-5}$ cm^2 s^{-1}; $\nu = 5.8 \times 10^{-5}$ cm^2 s^{-1}; 200 rpm; $N_{ad}^{max} = 4 \times 10^{14}$ cm^{-2}; $\theta = 1$; $k_c^- = 1.21 \times 10^{-7}$ cm^3 s^{-1}; $k_c^+ = 0$ cm^3 s^{-1}; and $R_s = 44.7$ Ω.

With $k_c^+ = 0$ cm^3 s^{-1}, we assume a perfect rectifying diode behavior which is in agreement with the experimental result: the saturation current density at 0.4 V ($\phi_{sc} = 1.242$ V) amounts to 30 nA cm^{-2}. For a rotation velocity of 200 rpm, the diffusion-limited current amounts to $I_{F,dl} = -7.1 \times 10^{-5}$ A.

References and Notes

(1) Diol, S. J.; Poles, E.; Rosenwaks, Y.; Miller, R. J. D. *J. Phys. Chem.* **1998**. In press.

(2) Meier, A.; Kocha, S. S.; Hanna, M. C.; Nozik, A. J.; Siemoneit, K.; Reineke-Koch, R.; Memming, R. *J. Phys. Chem. B.* **1997**, *101*, 7038.

(3) Miller, R. D. J.; McLendon, G.; Nozik, A. J.; Schmickler, W.; Willig, F. *Surface Electron-Transfer Processes*; VCH Publishers: New York, 1995.

(4) Lewis, N. S. *J. Phys. Chem.* **1998**, *102*, 4843.

(5) Fajardo, A. M.; Lewis, N. S. *J. Phys. Chem. B.* **1997**, *101*, 11136.

(6) Pomykal, K. E.; Lewis, N. S. *J. Phys. Chem. B* **1997**, *101*, 2476.

(7) Fajardo, A. M.; Lewis, N. S. *Science* **1996**, *274*, 969.

(8) Pomykal, K. E.; Fajardo, A. M.; Lewis, N. S. *J. Phys. Chem.* **1996**, *100*, 3652.

(9) Royea, W. J.; Fajardo, A. M.; Lewis, N. S. *J. Phys. Chem. B* **1997**, *101*, 11152.

(10) Lewis, N. S. *Annu. Rev. Phys. Chem.* **1991**, *42*, 543.

(11) Gu, Y.; Waldeck, D. H. *J. Phys. Chem.* **1996**, *100*, 9573.

(12) Wang, D.; Buontempo, J.; Li, Z. W.; Miller, R. J. D. *Chem. Phys. Lett.* **1995**, *232*, 7.

(13) Rosenwaks, Y.; Thacker, B. R.; Ahrenkiel, R. K.; Nozik, A. J. *J. Phys. Chem.* **1992**, *96*, 10096.

(14) Ellingson, R. J.; Asbury, J. B.; Ferrere, S.; Ghosh, H. N.; Sprague, J.; Lian, T.; Nozik, A. J. *J. Phys. Chem.* **1998**, *102*, 6455.

(15) Tachibana, Y.; Moser, J. E.; GrÄtzel, M.; Klug, D. R.; Durrant, J. R. *J. Phys. Chem.* **1996**, *100*, 20056.

(16) Hannappel, T.; Burfeindt, B.; Storck, W.; Willig, F. *J. Phys. Chem. B* **1997**, *101*, 6799.

(17) Moser, J. E.; Noukakis, D.; Bach, U.; Tachibana, Y.; Klug, D. R.; Durrant, J. R.; Humphry-Baker, R.; GrÄtzel, M. *J. Phys. Chem. B* **1998**, *102*, 3649.

(18) Fessenden, R. W.; Kamat, P. V. *J. Phys. Chem.* **1995**, *99*, 12902.

(19) Heimer, T. A.; Heilweil, E. J. *J. Phys. Chem. B* **1997**, *101*, 10990.

(20) Lanzafame, J. M.; Miller, R. J. D.; Muenter, A. A.; Parkinson, B. A. *J. Phys. Chem.* **1992**, *96*, 2820.

(21) Boudreaux, D. S.; Williams, F.; Nozik, A. J. *J. Appl. Phys.* **1980**, *51*, 2158.

(22) Nozik, A. J.; Memming, R. *J. Phys. Chem.* **1996**, *100*, 13061.

(23) Ross, R. T.; Nozik, A. J. *J. Appl. Phys.* **1982**, *53*, 3813.

(24) Marcus, R. A. *J. Phys. Chem.* **1990**, *94*, 4152.

(25) Marcus, R. A. *J. Phys. Chem.* **1990**, *94*, 7742.

(26) Smith, B. B.; Halley, J. W.; Nozik, A. J. *Chem. Phys.* **1996**, *205*, 245.

(27) Taube, H. *Electron-Transfer Reactions of Complex Ions in Solution*; Academic Press: New York, 1970.

(28) Koval, C. A.; Austermann, R. L.; Turner, J. A.; Parkinson, B. A. *J. Electrochem. Soc.* **1985**, *132*, 613.

(29) Herrmann, C.; Perault, G.; Pilla, A. *Anal. Chem.* **1968**, *56*, 1173.

(30) Buttry, D. A.; Ward, M. D. *Chem. Rev.* **1992**, *92*, 1355.

(31) Shimazu, K.; Yagi, I.; Sato, Y.; Uosaki, K. *Langmuir* **1992**, *8*, 1385.

(32) We note that some QCM experiments that were performed with aged, unsublimed and sublimed $Co(Cp)_2^0$ crystals from Aldrich did not show any response (i.e., mass change). NMR studies on these sublimed chemicals reveal that the $Co(Cp)_2^0$ crystals from Aldrich contained a higher concentration, as well as different impurities, than the $Co(Cp)_2^0$ from Strem. However, these impurities are believed to be of an organic nature because the electrochemical analysis at a gold electrode did not reveal any differences between solutions of the two $Co(Cp)_2^0$ sources.

(33) Cooper, J. B.; Bond, A. M. *Anal. Chem.* **1993**, *65*, 2724.

(34) Ward, M. D.; Lee, W. W.; White, H. S. *J. Am. Chem. Soc.* **1993**, *65*, 3232.

(35) Giles, C. H.; D'silva, A. P.; Easton, I. A. *J. Colloid Interface Sci.* **1974**, *47*, 11.

(36) Heiland, W.; Gileadi, E.; Bockris, J. *J. Phys. Chem.* **1966**, *70*, 1207.

(37) Bard, A. J.; Faulkner, L. R. *Electrochemical Methods*; John Wiley & Sons: New York, 1980.

(38) According to the model, ΔI_F can be considered as being decoupled from ΔI_C as long as surface concentrations of the redox system are equal to the bulk concentrations ($c_{redox}^s = c_{redox}^b$, $\Delta c_{redox}^s = 0$). This is in general the case if the faradaic current does not exceed ≈10% of the diffusion-limited current.

(39) Equation 23 for the total impedance Z is not quite complete to describe the impedance of the whole electrochemical setup. For this a series resistance R_s has to be added that takes into account the frequency and potential independent resistivity of the electrolyte solution and the external circuit, i.e., the impedance of the whole electrochemical setup is $R_s + Z$.

(40) Rhoderick, E. H.; Williams, R. H. *Metal-Semiconductor Contacts*; Clarendon Press: Oxford, 1988.

(41) Ashcroft, N. W.; Mermin, N. D. *Solid State Physics*; W. B. Saunders Company: New York, 1976.

(42) Nielson, R. M.; McManis, G. E.; Golovin, M. N.; Weaver, M. J. *J. Phys. Chem.* **1988**, *92*, 3441.

(43) Nielson, R. M.; McManis, G. E.; Weaver, M. J. *J. Phys. Chem.* **1989**, *93*, 4703.

(44) McManis, G. E.; Nielson, R. M.; Gochev, A.; Weaver, M. J. *J. Am. Chem. Soc.* **1989**, *111*, 5533.

(45) The reason that the slopes of the curves for the flatband and the surface redox potential are not exactly identical is due to the fact that during the long stationary measurements the solvent partially evaporates. This led to an increase of redox concentration (between 10% and 20%) with time and to an increase of the diffusion limited current. For the calculation of the surface redox potential with eq 18 the value of the diffusion limited current has to be known the more exactly the closer the ratio of $I_F/I_{F,dl}$ approaches unity. This time-dependent concentration change (or increase of the diffusion-limited current) can be proven by starting the measurement at negative potentials instead of starting in the depletion region.

(46) Memming, R. *Topics in Current Chemistry*; Springer-Verlag: Berlin, 1994; Vol. 169, p 106.

(47) Ba, B.; Cachet, H.; Fotouhi, B.; Gorochov, O. *Electrochim. Acta* **1992**, *37*, 309.

(48) Ba, B.; Fotouhi, B.; Gabouze, N.; Gorochov, O.; Cachet, H. *J. Electroanal. Chem.* **1992**, *334*, 263.

(49) Ba, B.; Cachet, H.; Fotouhi, B.; Gorochov, O. *J. Electroanal. Chem.* **1993**, *351*, 337.

(50) Ba, B.; Cachet, H.; Fotouhi, B.; Gorochov, O. *Semicond. Sci. Technol.* **1994**, *9*, 1529.

(51) The value for the kinematic viscosity of $\nu = 5.8 \times 10^{-3}$ cm^2 s^{-1} is an interpolated value between $\nu = 5.8 \times 10^{-3}$ cm^2 s^{-1} (21 °C) measured for an ACN−0.5 M $TBAPF_6$ solution and $\nu = 4.9 \times 10^{-3}$ cm^2 s^{-1} (21 °C) for an ACN−0.1 M $TBAPF_6$ solution. The kinematic viscosity for ACN as calculated from the viscosity and the density amounts to $\nu = \eta/\rho = 4.3 \times 10^{-3}$ cm^2 s^{-1} (Handbook of Chemistry and Physics, 74th ed.; CRC Press: Boca Raton, FL, 1993−1994).

(52) Landsberg, R.; Thiele, R. *Electrochim. Acta* **1966**, *11*, 1243.

(53) Scheller, F.; MÜller, S.; Landsberg, R.; Spitzer, H.-J. *J. Electroanal. Chem.* **1968**, *19*, 187.
(54) Scheller, F.; Landsberg, R.; MÜller, S. *J. Electroanal. Chem.* **1969**, *20*, 375.
(55) Smith, B. B.; Nozik, A. J. *Chem. Phys.* **1996**, *205*, 47.
(56) Smith, B. B.; Nozik, A. J. *J. Phys. Chem.* **1997**, *101*, 2459.
(57) Becke, A. D. *J. Chem. Phys.* **1993**, *98*, 1372.
(58) Becke, A. D. *J. Chem. Phys.* **1993**, *98*, 5648.
(59) Perdew, J. P. In *Electronic Structure Theory of Solids*; Ziesche, P., Eshrig, H., Eds.; Akademie Verlag: Berlin, 1991.
(60) Perdew, J. P.; Chevary, J. A.; Vosko, S. H.; Jackson, K. A.; Pederson, M. R.; Singhm, D. J.; Fiolhais, C. *Phys. Rev. B* **1992**, *46*, 6671.
(61) Becke, A. D. *Phys. Rev. A.* **1988**, *38*, 3098.
(62) Schrodinger, Inc. Jaguar, version; 3.0; Portland, OR, 1997.
(63) Qian, G.; Martin, R. M.; Chadi, D. J. *Phys. Rev. B.* **1988**, *37*, 1303.
(64) Biegelsen, D. K.; Bringans, R. D.; Northrup, J. E.; Swartz, E. L. *Phys. Rev. B.* **1990**, 5701.
(65) Qian, G.; Martin, R. M.; Chadi, D. J. *Phys. Rev. B* **1988**, *38*, 7649.
(66) Johnson, M. A.; Stefanovich, E. V.; Truong, T. N. *J. Phys. Chem.* **1998**. In press.
(67) Marcus, R. A. *Annu. Rev. Phys. Chem.* **1964**, *15*, 155.
(68) Gerischer, H. Z. *Phys. Chem. N. F.* **1961**, *27*, 40.
(69) Smith, B. B.; Nozik, A. J. To be published.
(70) In another previous publication (Rosenwaks, Y.; Thacker, B. R.; Nozik, A. J.; Ellingson, R. J.; Burr, K. C.; Tang, C. L. *J. Phys. Chem.* **1994**, *98*, 2739) ultrafast rate constants were also reported for photoinduced ET at p-InP in contact with $Fe(CN)_6^{4-/3-}$ in aqueous electrolyte when large electric fields were produced in the semiconductor space charge layer. The S_{ET} values were reported to show an electric field dependence, and they increased from about 10^4 cm/s to 5×10^7 cm/s as the band bending in the space charge layer increased from <0.1 to >0.5 eV. However, additional experimental studies of this system (Ellingson, R. J.; Nozik, A. J. Unpublished data.) showed a very pronounced dependence of the PL decay characteristics and its reversibility (with respect to the presence or absence of applied potential) on sample history and whether the laser excitation spot was stationary or moving during the experiment. With the laser spot moving, the PL decay was reversible; however, if the laser spot were stationary, then the fast PL decay with applied negative potential became constant and independent of potential. This indicates that some irreversible chemical changes are occurring at the p-InP surface with applied negative potential in the presence of $Fe(CN)_6^{4-/3-}$. Thus, the conclusions in this manuscript that a field dependence of the ET rate constant was observed and that ultrafast interfacial ET rates occurred at high fields are not supported by new data.
(71) Ahrenkiel, R. K. Minority-Carrier Lifetime in III−V Semiconductors. In *Minority Carriers in III−V Semiconductors: Physics and Applications*; Ahrenkiel, R. K., Lundstrom, M. S., Eds.; Academic Press: San Diego, 1993; Vol. 39, p 39.
(72) Rosenwaks, Y.; Shapira, Y.; Huppert, D. *Appl. Phys. Lett.* **1990**, *57*, 2552.
(73) Macdonald, J. R. *Impedance Spectroscopy*; John Wiley & Sons: New York, 1987.
(74) Gabrielli, C. Identification of electrochemical processes by frequency response analysis. Schlumberger Technologies Technical Report Number 004/83; Solartron/Schlumberger Instruments, Farnborough, England, 1984.
(75) Uhlendorf, I. Thesis, University of Hamburg, 1994.
(76) Uhlendorf, I.; Reineke-Koch, R.; Memming, R. *J. Phys. Chem.* **1996**, *100*, 4930.